Photometric characterization of a light source used for the absolute calibration of the fluorescence telescopes of the Pierre Auger Observatory

Bachelor-Thesis

zur Erlangung des akademischen Grades
Bachelor of Science (B.Sc) Physik

BERGISCHE UNIVERSITÄT WUPPERTAL

Fakultät 4 - Mathematik und Naturwissenschaft
Der Fachgruppe Physik vorgelegt von

Tobias Heibges
1621483

Wuppertal, 11. September 2019

1. Gutachter
Prof. Dr. Karl-Heinz Kampert

2. Gutachter
Prof. Dr. Christian Zeitnitz

Betreuer
Dr. Eric Mayotte

Contents

List of Figures

List of Tables

1. Introduction

The aim of this work is to give an absolute calibration for a lambertian light source within an uncertainty of 5%. An integrating sphere, built by Labsphere (3P-GPS-053-SL) [9], is used as a light source. This source was chosen as it will be used as the light source of the new XY-Scanner calibration system for the Fluorescence detectors of the Pierre Auger Observatory in Argentina.

The source itself consists of an integrating sphere equipped with three Roithner LaserTechnik UVLED365-110E UV-LEDs [15]. These LEDs are controlled by a single board computer (SBC) designed at KIT in Karlsruhe.

For the absolute calibration of the source, a Hamamatsu S1337-1010BQ photodiode [6] is used together with a Hamamatsu R9420-100 photomultiplier (PMT) [5] mounted on a passive base and supplied by a CEAN high voltage unit [4]. The current produced by the photodiode when illuminated is measured by a Keithley 6485 picoamperemeter [8], while the PMT voltage is recorded with a 6402 Picoscope [12].

In the source calibration measurement, the LEDs are flashed at a known rate with a pulse length of $5\,\mu$s, while the current running through the LEDs is changed between 1 mA and 20 mA. By flashing at different LED currents and measuring the resulting current on the photodiode, while monitoring the pulse stability with the PMT, a calibration curve can be extracted which can be used to convert the source settings into the photon count per pulse which can then be used to calibrate the Observatory.

Since the resolution of the Keithley 6485 picoamperemeter is not fine enough to record individual pulses, the source is pulsed at a high frequency so that the diode current can be measured in DC mode. Then the much higher timing resolution of the PMT is used to record individual pulses themselves.

To achieve the 5% uncertainty goal, this procedure must be performed in a well constrained environment. Therefore, the measurement is done in an electromagnetically shielded dark box and is geometrically constrained using precision machined brackets and 3D printed mounts for the sphere, PMT and photodiode.

2. Pierre Auger Observatory

The Pierre Auger Observatory is an international project involved in cosmic ray research. It is set up to detect very high energy cosmic rays with energies ranging from 10^{15} eV to 10^{21}eV. It is an indirect detector meaning single cosmic ray primaries are detected through the secondary particles created in interactions in the atmosphere which in turn can create new particles. This cascade of particles that develops in the atmosphere is called an extensive air shower and can be detected both through the particles that reach the ground and through the light the shower emits in the atmosphere.

At the Pierre Auger Observatory the detection of these air showers is split into two parts. There are the surface detectors (SD) which are mainly water tanks searching the Cerenkov light that is created when high energy particles pass through their water reservoir. In total there are 1660 surface detectors distributed over a surface area of 3000 km^2. In addition to the SD, there are the fluorescence detectors (FD) which look for the UV fluorescence light produced by charged particles in the air shower interacting with atmospheric nuclei. There are five FD telescope sites which house a total of 27 individual telescopes. The combination of SD and FD allows for a more accurate reconstruction of the energy, composition and incident direction of the primary particle. An example event detected by both the SD and FD can be seen in Figure 2.1.

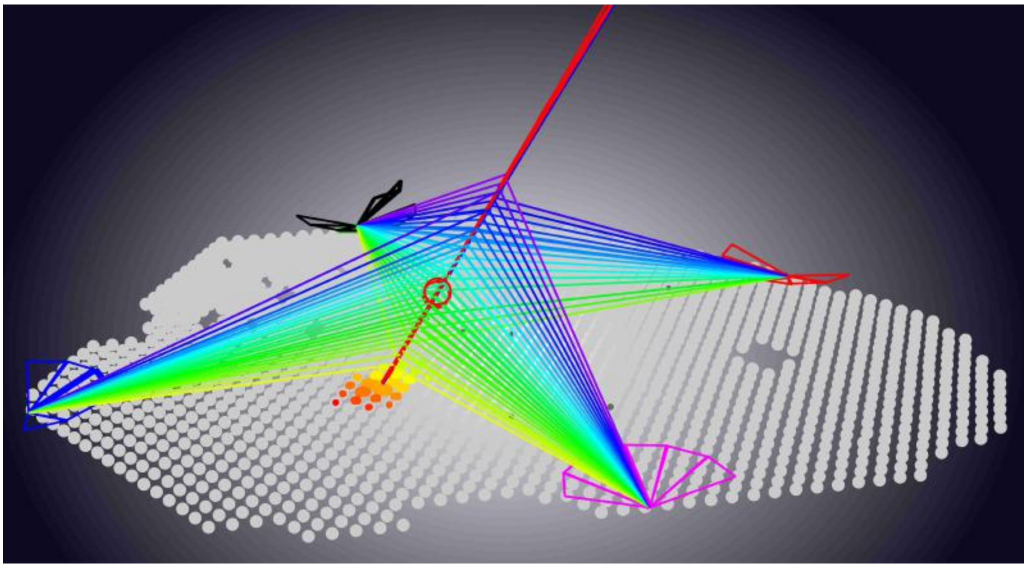

Figure 2.1.: *Map of the Pierre Auger Observatory with the SD in grey, and the FD as triangles. An example shower with the detection by the FD and SD can be seen. [2]*

This ability for the observatory to measure air showers with both the FD and SD makes it a hybrid detector. This is useful, since the amount of fluorescence light emitted by an air shower is directly proportional to the energy of the incident particle meaning the FD allows for a direct measurement of the primary particle's energy. In events which are measured with both SD and FD, this FD energy can be used to calibrate the SD response. For this reason the energy resolution of the FD telescopes sets the energy resolution of the full observatory and therefore needs an absolute calibration that is as precise as possible.

The fluorescence telescopes are primarily a camera consisting of an array of 440 PMTs and a large mirror. Light from the shower first passes through a UV filter which only allows light with wavelength between ∼330-385 nm to pass. This light is then is directed onto the PMTs using a large segmented spherical mirror. This set up leads to each PMT having a 1.5° field of view on the sky. Using the data from the individual PMTs it is then possible to record the development of the air shower in the atmosphere. A sketch of the set up can be seen in Figure 2.2a.

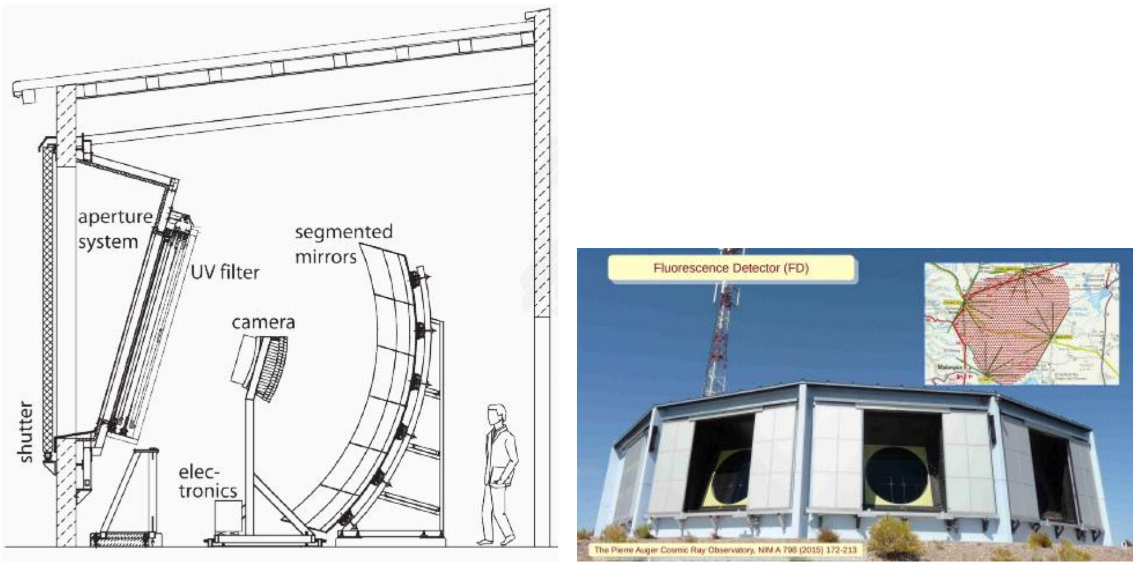

(a) *Sketch of the FD set up [2]* ***(b)*** *Telescope [2]*

Figure 2.2.: *Figure (a) shows a sketch of the FD telescope. Figure (b) shows a outside picture of the telescope house.*

There are frequent relative calibrations of the FDs which use LEDs as a light source in the set up. Unfortunately, these LEDs degrade and change over time. For this reason a absolute calibration is necessary to reset the energy scale of the FDs. Before, this was done by using a big diffuse light source housed in a drum with a diameter of 2.5 m that was placed on top of the UV filter in front of the mirrors. Using the ratio of the light intensity of the drum and the height of PMT signals, an absolute calibration was performed with an end to end uncertainty of 9%. This calibration was very difficult to perform and took up a lot of man power and time which lead to infrequent and expensive calibrations. Therefore, the drum calibrations were only done in 2004, 2010 and 2013 and have not been performed since. To remove the high manpower and time costs, the XY-Scanner is currently being developed and tested.

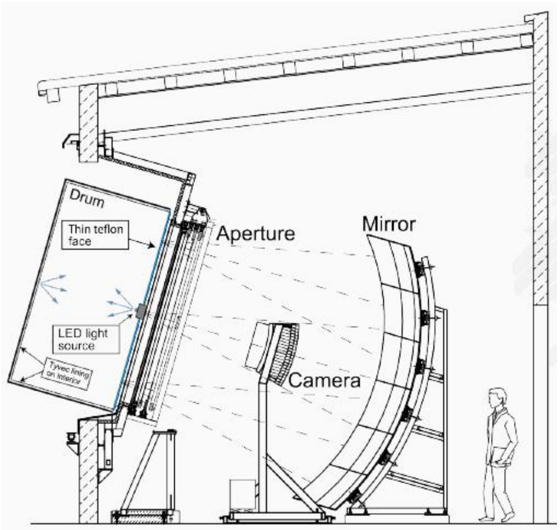

(a) *Sketch of drum calibration [2]*

(b) *Picture of the drum calibration [16]*

Figure 2.3.: *Figure (a) shows a sketch of the drum calibration. Figure (b) shows a picture of the drum calibration being performed on an FD telescope.*

Overall, the XY-Scanner method aims to improve the measurement frequency by making the calibration quicker and possible with less man power than the drum calibration, and in an ideal case, potentially the calibration can be completely automated. It consists of an integrating sphere which can be moved across the whole surface of the aperture and flashes at several points. The advantage of having a small light source, other than being easier to handle, is that the absolute calibration of its uniformity and emission intensity is much less prone to error than the large 2.5 m source. A sketch of the planned set up is shown in Figure 2.4. The basic idea is that if there are enough points at which the source is flashed, then the illuminated regions overlap and give a similar calibration result as the old drum calibration.

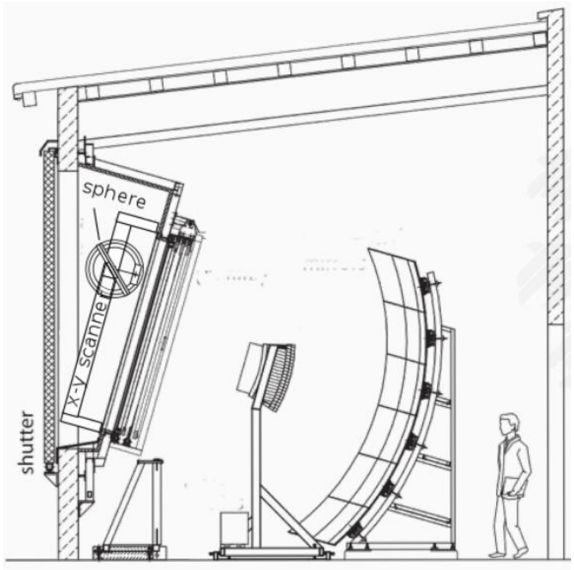

Figure 2.4.: *Sketch of the XY Scanner set up on the Fluorescence telescopes. [10]*

In this work, the absolute calibration of the integrating sphere from Labsphere is performed, which is the same source as for the XY-Scanner. This absolute calibration will in turn be used to provide a preliminary absolute calibration for the Pierre Auger Observatory FD.

3. Conversion

In the following, an equation that converts the current measured on the diode, I_{diode}, into a photon count per pulse, N_γ, is derived.

The illumination power at the diode is related to the current produced as

$$P = \frac{I_{\text{diode}}}{\eta_{\text{diode}}}, \tag{3.1}$$

where η_{diode} is the efficiency of the diode at a given wavelength. Since the power is energy per time and the energy of a single photon is given by $E = h\nu$, the photon flux Φ_{diode} at the diode can be calculated as

$$\begin{aligned} P = \frac{E}{t} = \frac{N_{\gamma,\text{diode}} \cdot h \cdot \nu}{t} &= h \cdot \nu \frac{N_{\gamma,\text{diode}}}{t} = h \cdot \nu \cdot \Phi_{\text{diode}} \\ \Rightarrow \Phi_{\text{diode},1\,\text{s}} = \frac{I_{\text{diode}}}{\eta_{\text{diode}} \cdot h \cdot \nu} &= \frac{I_{\text{diode}}}{\eta_{\text{diode}} \cdot h \cdot \frac{c}{\lambda}} = \frac{I_{\text{diode}}\lambda}{\eta_{\text{diode}} \cdot h \cdot c}. \end{aligned} \tag{3.2}$$

The equation 3.2 can now be used to convert the current measured to a number of photons hitting the diode per second. To get the flux per pulse, this equation is divided by the flashing frequency f

$$\Phi_{\text{diode}} = \frac{I_{\text{diode}}\lambda}{f \cdot \eta_{\text{diode}} \cdot h \cdot c}. \tag{3.3}$$

3.1. Efficiency

Since the efficiency of the diode is of crucial importance to the conversion calculation it is necessary to find the value that describes the response of the diode to the light output of our LEDs.

This is done using the calibration provided by Hamamatsu which connects the output current to the power incident on the diode and is shown in Figure 3.1. According to Hamamatsu this calibration has an accuracy of 2%. In the future, a NIST (or similar) calibration will be used with an uncertainty of less than 1%.

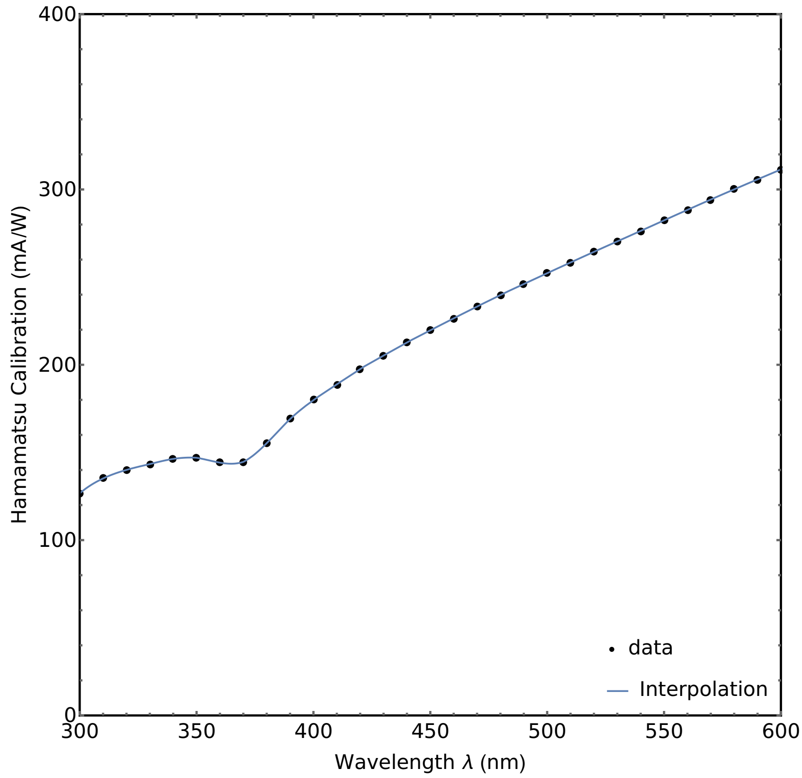

Figure 3.1.: *This figure shows the Hamamatsu efficiency calibration depending on the wavelength. Since the calibration was done on discrete points an interpolation curve created by Mathematica [7] was produced for subsequent calculations.*

The LEDs used inside the sphere produce light with the spectrum shown in Figure 3.2. Unfortunately, the exact function describing the spectrum was not provided which is why it was necessary to extract points from the plot and fit an interpolation curve. The data extraction was done using the online plot converter "WebPlotDigitizer 4.2" [14]. The resulting data points were used to create an interpolation function using Mathematica that describes the spectrum with minimal error.

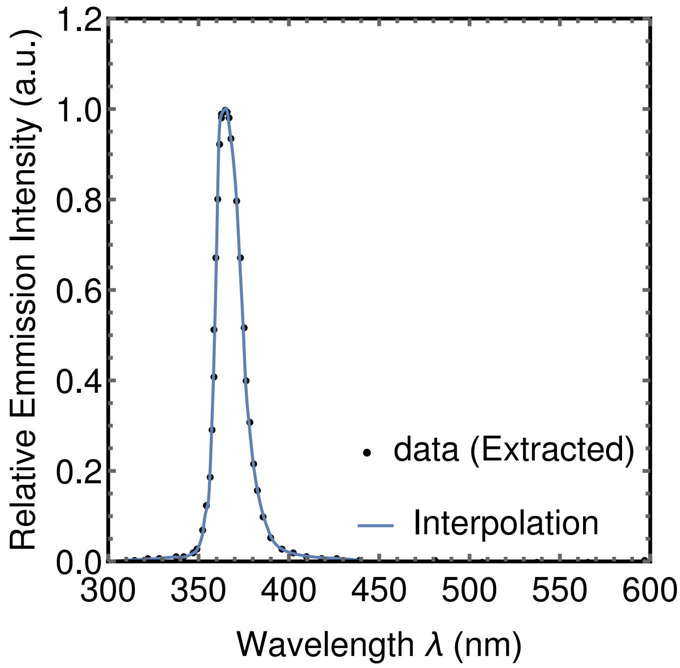

Figure 3.2.: *This figure shows the digitized LED spectrum together with an interpolation function created by Mathematica.*

The spectrum defined by the interpolation function can now be folded onto the efficiency curve via

$$\frac{1}{A}\int_{300}^{600} \eta_{\text{diode}}(\lambda) \cdot \Phi(\lambda) d\lambda = \eta_{\text{diode,eff}} \tag{3.4}$$

where A is the integral of the spectrum, $\eta_{\text{diode}}(\lambda)$ is the efficiency interpolation and $\Phi(\lambda)$ is the interpolated LED spectrum. The integrals are carried out from 300 to 600 nm to give a final value for the efficiency of

$$\eta_{\text{diode,eff}} = 147.1\,\frac{\text{mA}}{\text{W}}. \tag{3.5}$$

3.2. Flux from sphere

The fraction of the photon flux emitted from the sphere which reaches the photodiode can be calculated using the lambertian light distribution. The lambertian light distribution assumes that every point of the emitting surface is radiating light isotropically with the same brightness. With these assumptions, light emitted from a differential emitting area dA into a differential solid angle $d\Omega$ is given by

$$\Phi_{target} = \Phi_{emitted} \cdot \cos(\theta) d\Omega dA. \tag{3.6}$$

This corresponds to the light distribution shown in Figure 3.3

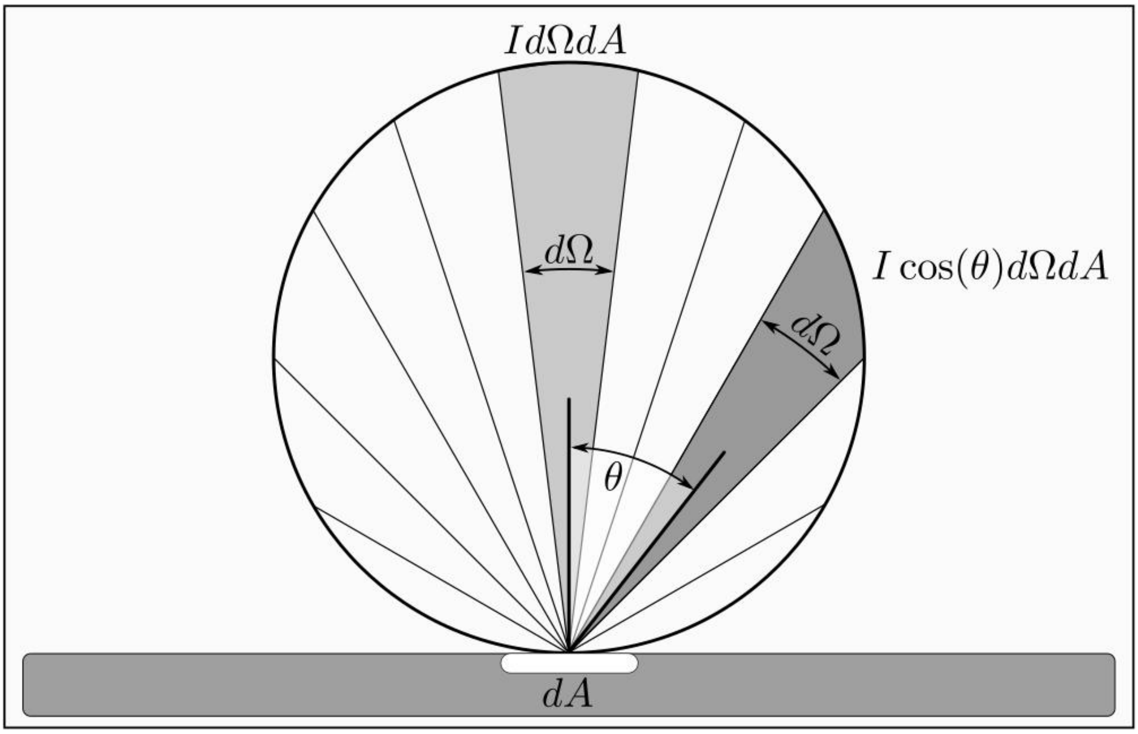

Figure 3.3.: *Lambertian light distribution and light intensity radiated into the solid angle* $d\Omega$

Extending this treatment to non differential areas leads to the following integral equation

$$\Phi_{diode} = \int\int \Phi_{Sphere}\cos(\theta)d\Omega dA = \Phi_{Sphere}\int\int \cos(\theta)d\Omega dA, \tag{3.7}$$

where $d\Omega$ describes the solid angle of the photodiode as seen from the outlet of the sphere. dA is an infinitesimal part of the area of the sphere outlet.

The specific integral that needs to be solved is defined by the geometric configuration shown in Figure 3.4 and ends up being difficult to evaluate.

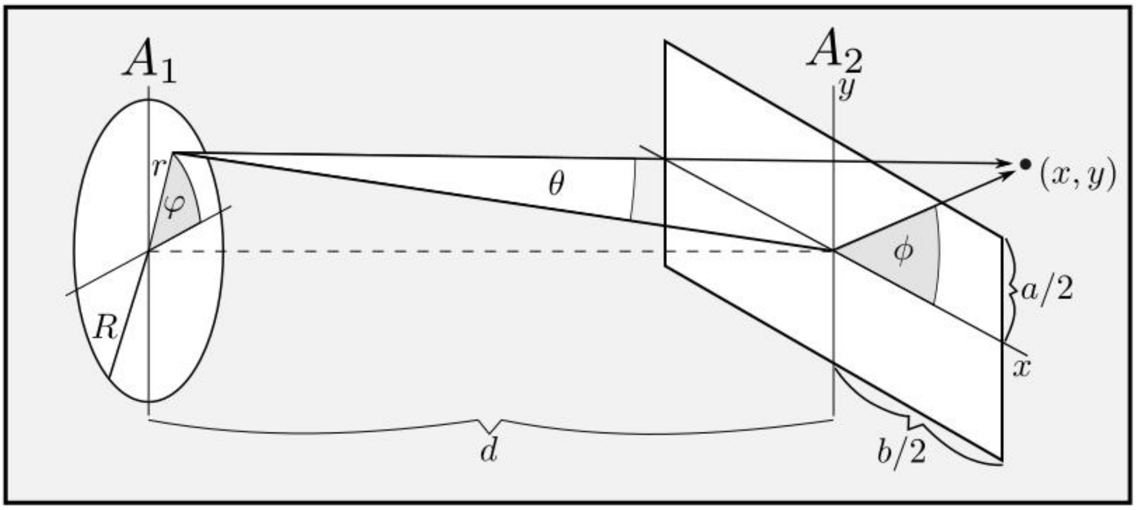

Figure 3.4.: *Geometric configuration of the setup.* A_1 *represents the sphere outlet and* A_2 *the diode*

3.2.1. View factor

Fortunately the relationship between surfaces emitting and receiving radiation with lambertian distributions is described by heat transfer equations, particularly the view factor which describes the fraction of radiation hitting the target divided by all the radiation that is emitted

$$F_{12} = \frac{\Phi_{diode}}{\Phi_{Sphere}} \tag{3.8}$$

which is an equivalent value to that in Equation 3.7.

According to [3] the view factor of a rectangle emitting light which strikes a coaxial disk is given by

$$F_{21} = 0.3252F_{2j}^{0.9137} + 0.6815 * F_{2k}^{1}.0568 \tag{3.9}$$

with

$$
\begin{aligned}
F_{2n} = & \frac{\log\left(\frac{\left(p^2+s^2+1\right)\left(q^2+\mathrm{r}^2+1\right)}{\left(p^2+\mathrm{r}^2+1\right)\left(q^2+s^2+1\right)}\right)}{\pi(p-q)(\mathrm{r}-s)} \\
& + \frac{2\sqrt{p^2+1}\left(\mathrm{r}\arctan\left(\frac{\mathrm{r}}{\sqrt{p^2+1}}\right) - s\arctan\left(\frac{s}{\sqrt{p^2+1}}\right)\right)}{\pi(p-q)(\mathrm{r}-s)} \\
& + \frac{2\sqrt{\mathrm{r}^2+1}\left(\mathrm{r}\arctan\left(\frac{p}{\sqrt{\mathrm{r}^2+1}}\right) - s\arctan\left(\frac{q}{\sqrt{\mathrm{r}^2+1}}\right)\right)}{\pi(p-q)(\mathrm{r}-s)} \\
& - \frac{2\sqrt{s^2+1}\left(\mathrm{r}\arctan\left(\frac{p}{\sqrt{s^2+1}}\right) - s\arctan\left(\frac{q}{\sqrt{s^2+1}}\right)\right)}{\pi(p-q)(\mathrm{r}-s)} \\
& - \frac{2\sqrt{q^2+1}\left(\mathrm{r}\arctan\left(\frac{\mathrm{r}}{\sqrt{q^2+1}}\right) - s\arctan\left(\frac{s}{\sqrt{q^2+1}}\right)\right)}{\pi(p-q)(\mathrm{r}-s)}
\end{aligned}
\tag{3.10}
$$

where $n \in \{j, k\}$ and using the following abbreviations

$$
\begin{array}{lllll}
R = \frac{r_{\text{Sphere}}}{d}; & W = \frac{a}{2d}; & L = \frac{b}{2d}; & & \\
\text{for } n = j & p = \frac{R}{\sqrt{2}+W}; & q = \frac{R}{\sqrt{2}-W}; & r = \frac{R}{\sqrt{2}+L}; & s = \frac{R}{\sqrt{2}-L}; \\
\text{for } n = k & p = R+W; & q = R-W; & r = R+L; & s = R-L.
\end{array}
$$

In the special case of our square photodiode the simplification $a = b$ can be applied which leads to the expression

$$
\begin{aligned}
F_{2n} = & \frac{1}{\pi(p-q)^2}\left(4\sqrt{p^2+1}\left(p\tan^{-1}\left(\frac{p}{\sqrt{p^2+1}}\right) - q\tan^{-1}\left(\frac{q}{\sqrt{p^2+1}}\right)\right)\right. \\
& \left. + 4\sqrt{q^2+1}\left(q\tan^{-1}\left(\frac{q}{\sqrt{q^2+1}}\right) - p\tan^{-1}\left(\frac{p}{\sqrt{q^2+1}}\right)\right) + \log\left(\frac{\left(p^2+q^2+1\right)^2}{\left(2p^2+1\right)\left(2q^2+1\right)}\right)\right)
\end{aligned}
$$

which uses the same definitions as before.

Using the reciprocity relation of the view factor, given by

$$
A_1 F_{12} = A_2 F_{21} \tag{3.11}
$$

the view factor for radiation emitted from the disk to the rectangle is given by

$$
F_{12} = \frac{A_2}{A_1} F_{21} \tag{3.12}
$$

Using this equation and plugging in the areas A_1 and A_2 the equation that converts the photon flux at the diode to the total flux leaving the sphere is given by

$$\Phi_{\mathrm{Sphere}} = \frac{r^2\pi}{a^2}\frac{\Phi_{\mathrm{diode}}}{F_{12}} \tag{3.13}$$

Equation 3.13 together with Equation 3.2 results in an equation that describes the photon flux leaving the sphere depending on the current measured on the diode.

$$\Phi_{\mathrm{Sphere}} = \frac{\pi r^2 \frac{I_{\mathrm{diode}}\lambda}{f\cdot\eta_{\mathrm{diode}}\cdot h\cdot c}}{a^2 F_{12}} = \frac{r^2 \cdot I_{\mathrm{diode}} \cdot \lambda}{a^2 \cdot F_{12} \cdot f \cdot \eta_{\mathrm{diode}} \cdot h \cdot c} \tag{3.14}$$

4. Hardware

The Flasher consists of an integrating sphere with three UV-LEDs which are controlled with a custom build Single Board Computer (SBC) called the flasherboard. The characteristics of the LEDs have already been discussed in section 3.1. A short summary of the main features of the integrating sphere and the flasherboard are given in the following chapter.

4.1. The Integrating Sphere

The light source primarily consists of an integrating sphere built by Labsphere. It has a inner diameter of 13.495 cm and is coated with Spectralon, a highly diffuse reflective coating, which when combined with the multiple reflections that light must travel to leave the sphere, results in a nearly isotropic lambertian light distribution as well as possible. Inside the sphere there are three Roithner LaserTechnik UV-LEDs that emit light with the spectrum shown in Figure 3.2. An interior baffle is positioned to prevent light emitted by the LEDs from directly leaving the sphere. For the calibration measurement only one LED is used, while the others are reserved for aging studies. The sphere port itself has a diameter of 2.5 in (6.35 cm) which is treated as the lambertian emission surface.

In Equation 3.13 the distance from the port to the diode plays an important role and a deviation of 1 mm corresponds to approximately 1% deviation in the calibration. Therefore the location of the lambertian surface in the outlet needs to be known accurately. Here, we assume that the lambertian surface lies at the inner most white rim of the sphere which can be seen in Figure 4.1a.

(a) *Rim of the Sphere* ***(b)*** *Front view*

Figure 4.1.: *Figure (a) shows the position of the rims and the naming used. Figure (b) shows the front view onto the sphere with the inner rim as the surface of last scattering.*

This assumption is based on the fact that when viewed from the front this rim is the last point of scattering before the light leaves the sphere as can be seen in Figure 4.1b.

As a point of reference the outer lip of the sphere is used to align the sphere in the setup. For this reason the distance between this lip and the inner white rim is measured at 16 points around the outlet with the results shown in Figure 4.2.

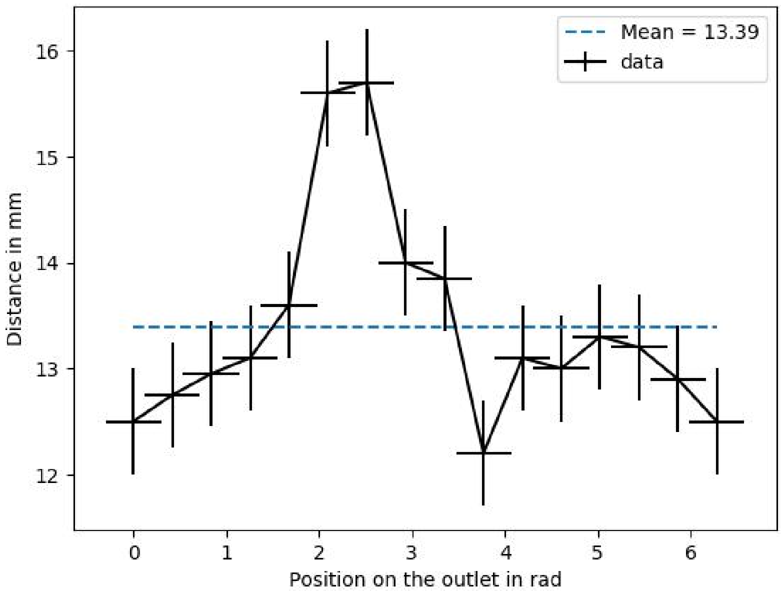

Figure 4.2.: *This figure shows the distance from the outer lip of the sphere to the white inner rim as defined in Figure 4.1a. All the measurements are taken to within 0.5 mm of accuracy.*

The sphere used in the test setup shows a very high fluctuation of up to 3 mm which results in a high contribution to the total error due to the uncertainty in the location of the lambertian surface. This issue with the sphere is however not seen in the sphere used in the field.

In the following the distances between the diode and the sphere is given by the mean value of this measurement with the error given by the standard deviation.

$$d_{\text{Lip to outlet}} = 13.4 \pm 1.0\,\text{mm} \tag{4.1}$$

4.2. Flasherboard

The LEDs inside the sphere are controlled using a flasherboard designed in Karlsruhe at KIT. It is a single board computer with three connections. One connection is to the power supply and the external trigger. The second is a connection to the LEDs that is used to send power for the LED pulses and to monitor the LED temperature. The third connection is on the internal photodiode mounted inside the sphere. A picture of the Flasher board is shown in Figure 4.3

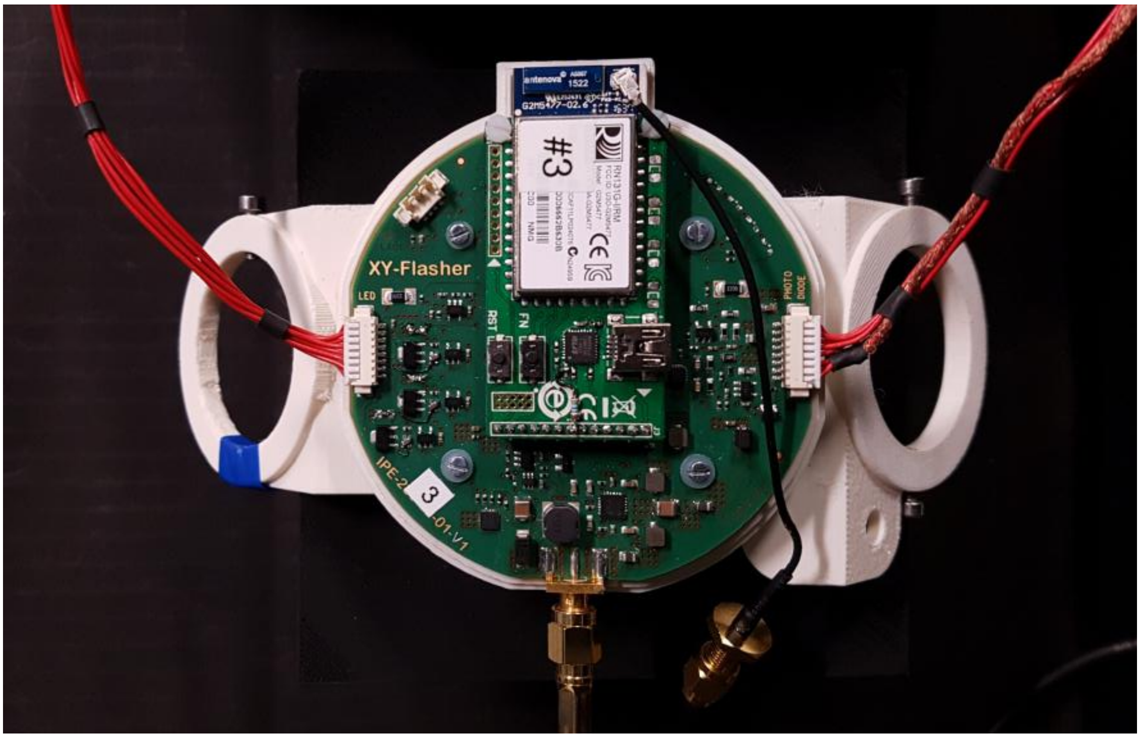

Figure 4.3.: *This figure shows the Flasher board with all three ports connected.*

The control of the flasher is done via software hosted on an external computer. The communication between the computer and the flasherboard takes place over a RN-131 wifi-card [17]. The wifi communication however leads to spikes in the recorded signals and therefore is a major source of noise in the measurements. To avoid this, the wifi signal is exported to an external antenna outside of the darkbox as can be seen in Figure 5.2c

5. Measurement

For the calibration measurement a calibrated Hamamatsu S1337-1010BQ photodiode and a Hamamatsu R9420 PMT are used. These are read out by a Keithley 6485 picoamperemeter and a 6402 Picoscope, respectively. The need for these two parts is explained in section 5.1 while the measurement set up of the diode, PMT and sphere are explained in section 5.2.

5.1. Method

The Keithley 6485 picoampermeter has a minimum integration time of $\sim 1\,\mathrm{ms}$. This poses a problem to the measurement since the maximum pulse length that can be produced is $\sim 20\,\mu\mathrm{s}$. In order to bridge this two order of magnitude time difference, the calibration is split into two parts.

The picoampermeter is used to measure a steady state current through the photodiode. To do this the integration time of the picoampermeter is set to a 0.5 s and the LEDs are flashed at a high rate. At a flashing rate of 100 Hz there are 50 flashes during the 0.5 s time period and the current measured by the picoampermeter approaches a steady state. The conversion of the steady state current to the current produced by one flash during this integration time is given by

$$I_{\text{flash}} = \frac{I_{\text{steady state}} - I_{\text{baseline}}}{f} \tag{5.1}$$

where f is the flashing frequency. When the efficiency of the photodiode is known, this single flash current and Equation 3.14 can be used to calculate the number of photons hitting the diode.

To get more detailed information about every single flash, the Hamamatsu PMT is used. This PMT has a rise time of just a few ns and is therefore able to measure the pulse shape of each flash very accurately. The PMT is connected to a 6402 Picoscope on which the voltage across a $50\,\Omega$ of resistance is measured. From these measurements information on the pulse length and pulse integral is extracted.

5.2. Test bench set up

The set up for this experiment has to meet the requirements motivated by the operation goals of the Pierre Auger Observatory of less than 5% calibration uncertainty. This requires that:

- The distance from the sphere to the photodiode is known to within 2 mm
- The photodiode is centered on the sphere output
- The PMT is at a fixed position with respect to the photodiode
- The reflections into the photodiode are small compared to the light directly from the source
- The set up is easy to build and operate for eventual use in Argentina.

A set up which aims to meet these requirements is sketched in Figure 5.1 and will be further elaborated in subsection 5.2.2.

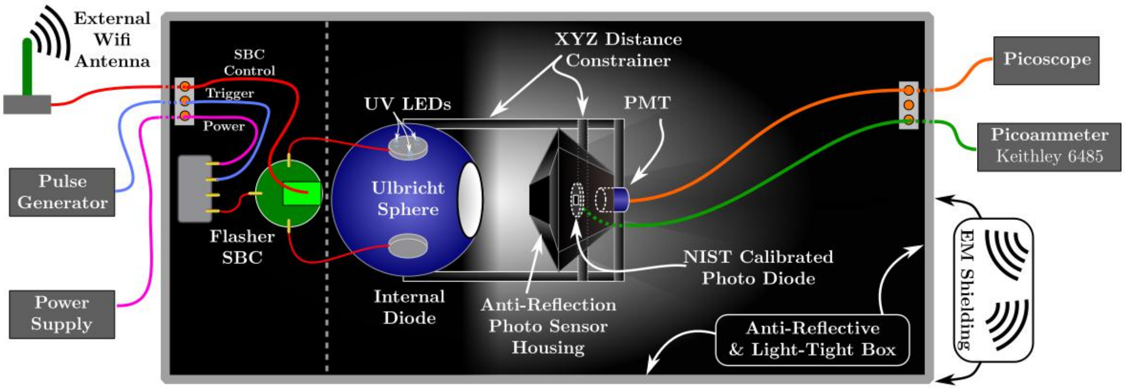

Figure 5.1.: This figure shows a sketch of the Calibration Bench.

5.2.1. Noise

In order to satisfy the requirements listed of a 5% uncertainty on the calibration, the set up needs to be shielded from all kinds of noise.

To do this, the setup is housed in the light tight box shown in Figure 5.2a. The box is grounded at several points, as can be seen in Figure 5.2b, to reduce the electromagnetic noise from the outside. To decrease the light noise from reflections inside the box, it is painted with a highly light absorbent paint.

To further decrease the electromagnetic noise, the wifi antenna of the flasherboard (see section 4.2) is exported to the outside of the box shown in Figure 5.2c and all status LEDs are desoldered or covered.

To further reduce the noise in the measurements, all signal cables are looped through farad rings as shown in Figure 5.2d

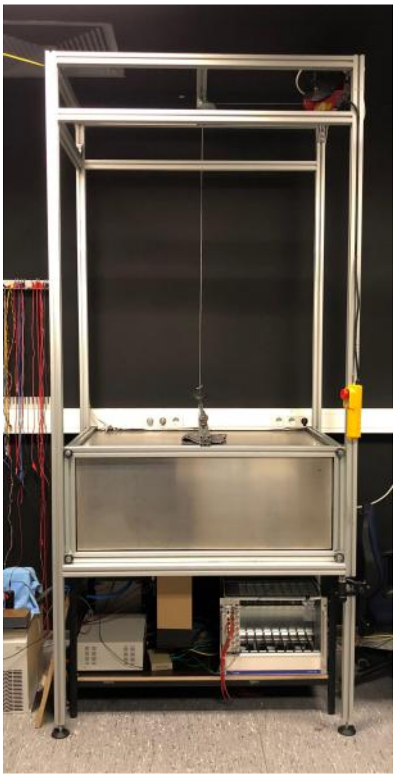

(a) Dark box

(b) Grounding

(c) Exporting the wifi signal

(d) Farad rings around signal cables

Figure 5.2.: *Figure (a) shows the dark box used in the experiment. Figure (b) shows the grounding of the box. Figure (c) shows the wifi being exported to an external antenna. Figure (d) shows the farad rings around the measurement cables.*

5.2.2. Alignment and distance constrains

To achieve the accuracy needed in the alignment of Sphere and diode, two different set ups were made.

Due to its easy operation, high customizability and high printing accuracy, the first attempt for the set up was entirely 3D printed. As can be seen in Figure 5.3, this set up allows for easy changes in the distance between the photodiode and the sphere. Because of the small crossbars and large shields it also allows only few opportunities for reflections into the diode.

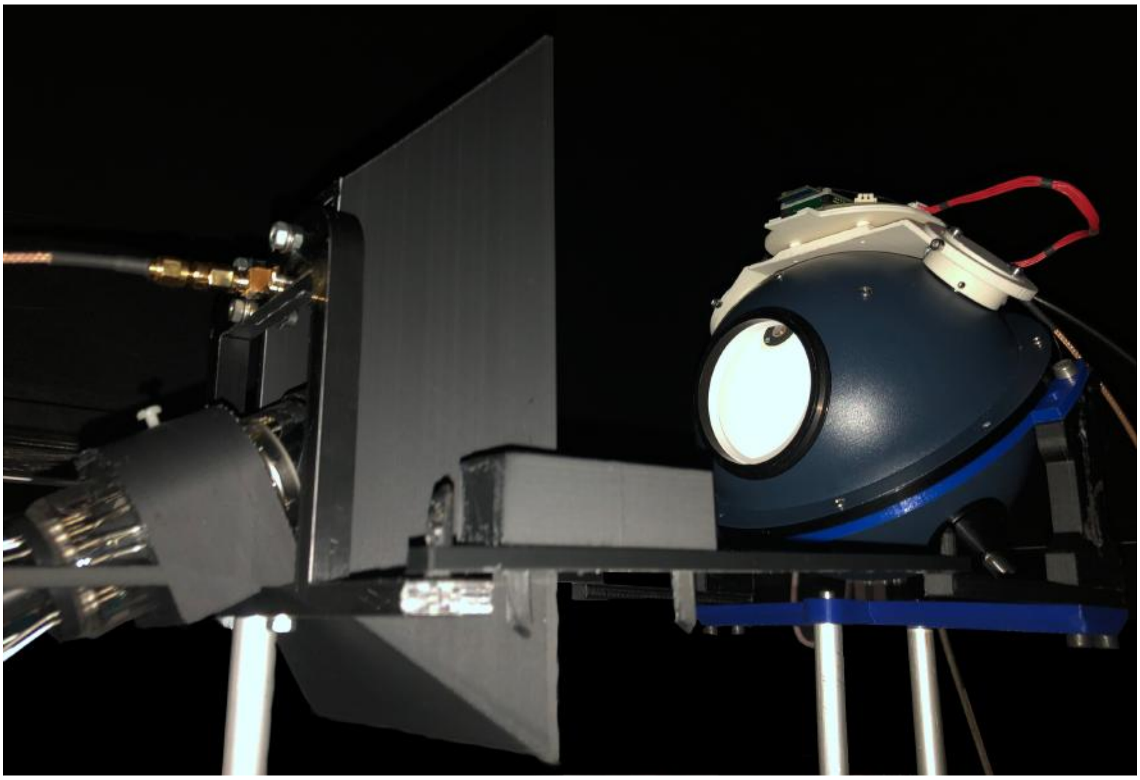

Figure 5.3.: *The figure shows the the first setup with the big anti reflection housing and the flasher looking at the diode. It allows only few reflections but is not rigid enough and shows a high length dependence with temperature.*

Unfortunately, the construction is not very rigid and could easily be tilted toward or away from the sphere. Apart from that, the PLA/ABS print material shows a high length variability of about 1% due to changes of temperature and/or humidity. At a total measurement length of at least 20 cm this leads to a distance uncertainty of > 2 mm or $\sim 2\%$. For this reason this setup had to be abandoned.

To avoid this uncertainty in the diode location the new design which is shown in Figure 5.4 was made. This set up is, in the most parts, constructed from off the shelf aluminum profiles precision machined to the desired lengths. The length variation of these profiles due to temperature and humidity is negligible, especially since the temperature for most measurements is held at a constant 25 °C by air conditioning. In this design, only the diode-/PMT-mount and the mount of the sphere are 3D printed since custom designs were needed. A sketch of this setup is shown in Figure 5.4.

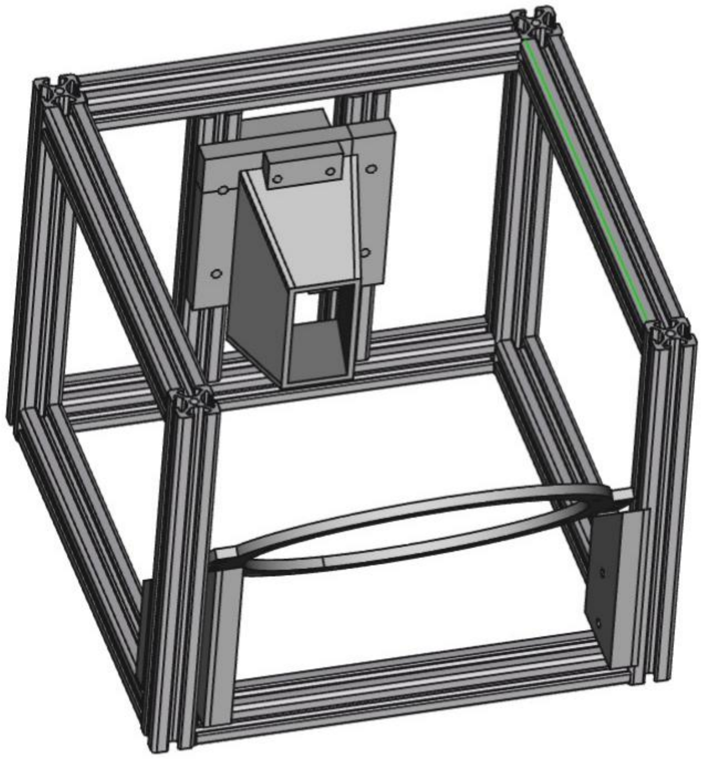

Figure 5.4.: *Final set up with item profiles. The integrating sphere is mounted inside the ring shown in the figure.*

This setup has the disadvantage of having much larger cross bars which can lead to more reflections in the diode. To counteract this, a more aggressive field of view constrainer was designed and printed which can also be seen in Figure 5.4. To further decrease reflections the whole set up is also coated with a highly light absorbent paint.

To ensure that the diode is centered on the port, a special sphere cap was printed that uses the same holes as the diode holder, which can be seen in Figure 5.5.

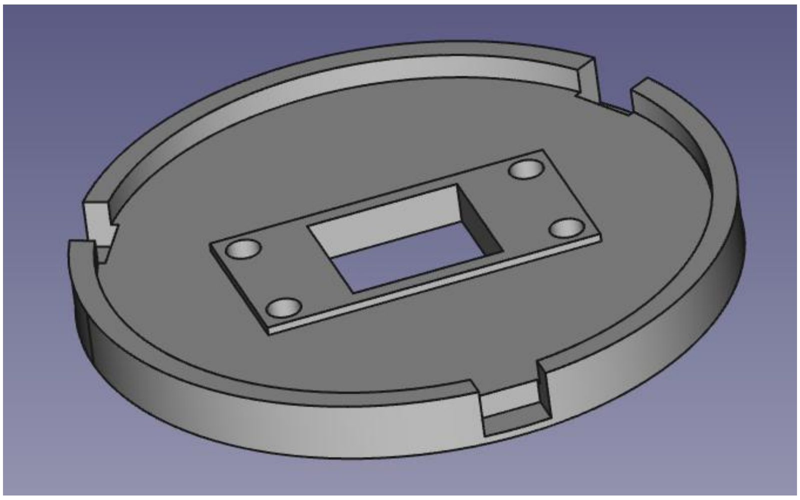

Figure 5.5.: This figure shows the cap that is used for the alignment of the diode and the sphere

This cap is secured to the diode holder and moved until it covers the sphere output. Proper alignment can be checked with the three indentations on the side through which one can see if the cap lies flat on the outer lip of the sphere. If this is the case then the diode is aligned at the center of the port.

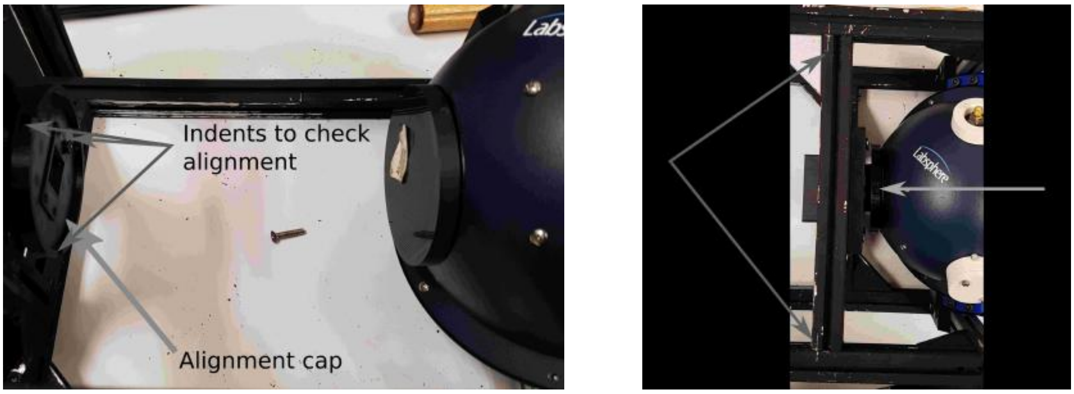

(a) *Alignment cap* **(b)** *Sphere aligned*

Figure 5.6.: *Figure (a) shows the alignment cap mounted on the diode holder. The three points to check the alignment can be seen. Figure (b) shows the aligned sphere. Scratches in the item profiles indicate the position relative to which the distance can be measured.*

Since the distance between the outer lip and the lambertian surface is known (see section 4.1) and the distance from the diode to the outer Lip in the aligned state is also known, it is possible to use the position at alignment, as shown in Figure 5.6b, as a reference point from which the distance between the diode and the sphere can be set in later measurements.

In total the uncertainty on the diode location is estimated to be about 2 mm in distance including the uncertainty in the location of the lambertian surface. The mis alignment is estimated to be <0.2 mm since the accuracy of the 3D printer is 0.1 mm and adding in a small extra margin to be conservative leads to this number.

5.3. Measurement Programs

In order to make the calibration as simple and fast as possible, all measurement are controlled via bash and python scripts. The measurement tasks are split into three major parts

- Control of the Flasher and HV
- Picoamperemeter measurement
- Picoscope measurement

To deal with each of these, three programs have been written: one running the picoamperemeter, one running the Picoscope and a bash control script that combines the control of the Flasher and HV and coordinates the measurements of the Picoscope and picoamperemeter. The SVN repository of the code used can be accessed via

git svn clone https://at-web.physik.uni-wuppertal.de/svn/AbsoluteCalibration

The picoamperemeter script uses RS-232 serial communication. The commands are based on the EPICS communication scripts [1] and can also be found in the Programmers Guide for the Keithley 6485 picoamperemeter. Most of the code for the Picoscope hosted in Picoscope.py was provided by Dr. Anna Pollmann [13], and only the last lines which define the measurement had to be changed.

The measurement is set up in a way so that the flasher will flash until the picoamperemeter has taken its measurements after which the picoamperemeter script will finish and the flasher is sent a stop command. One full measurement of 200 current readings takes about 5 min to complete. On the Picoscope the limiting factor on the number of possible measurements is the buffer size. At a sampling frequency of $1 \cdot 10^8$ samples per second and 1100 points per set, 2000 measurements are possible which at a flashing rate of 100 Hz takes about 20 s.

6. Analysis

The analysis is deeply connected with measurement concept presented in section 5.1. For this reason the analysis, just as the measurement itself, is split into two parts. The bulk of the absolute calibration itself is obtained via an analysis of the data from the photodiode. The uncertainties on the other hand are mainly calculated through a separate analysis of the data from the PMT.

6.1. Analysis of the diode data

From the diode there are two things needed. First the overall viability of the method described in section 5.1 will be checked in section 6.1.1. Then the derivation of a calibration constant which defines the sphere photon output at any given LED input current and pulse length will be presented in section 6.4.

6.1.1. Method validation

The validation measurement is performed over several different pulse lengths and pulse amplitudes. A linear increase in the input current should lead to an almost linear increase in the number of emitted photons and in turn to an increase in the diode current. The exact dependence as specified by Roithner LaserTechnik can be seen in the appendix Figure A.1. Likewise, an increase in the pulse length should also lead to a proportional increase in the diode current.

To test this, photodiode current measurements at several different LED currents and pulse lengths were made. As discussed earlier, the photodiode current to pulse amplitude and pulse length relationship should be close to linear. Figure 6.3 shows the measured dependence of the diode current on the pulse length at a constant LED current.

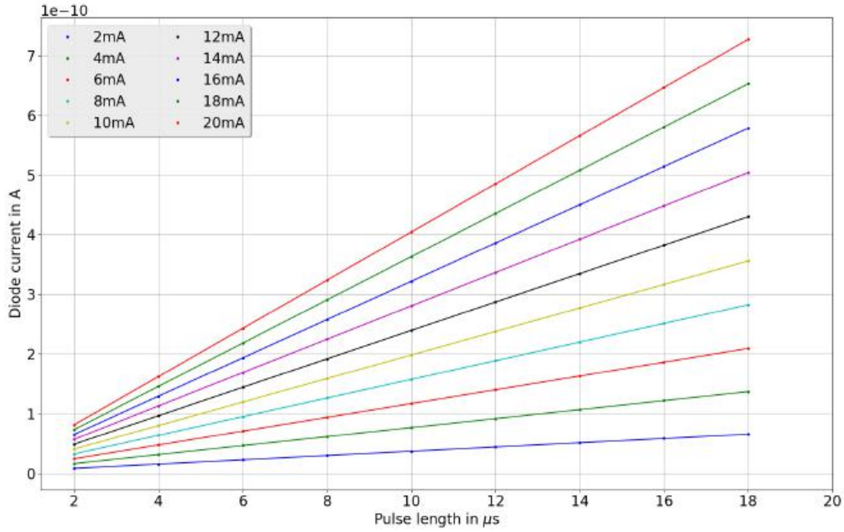

Figure 6.1.: *Full measurement on the dependence of the diode current on the pulse length at a constant input current. The measurements agree with the line fits very well.*

The data in Figure 6.1 shows a high agreement with the linear fits illustrated by the lines on the figure. This can also be seen when looking at the residuals shown in Figure 6.2.

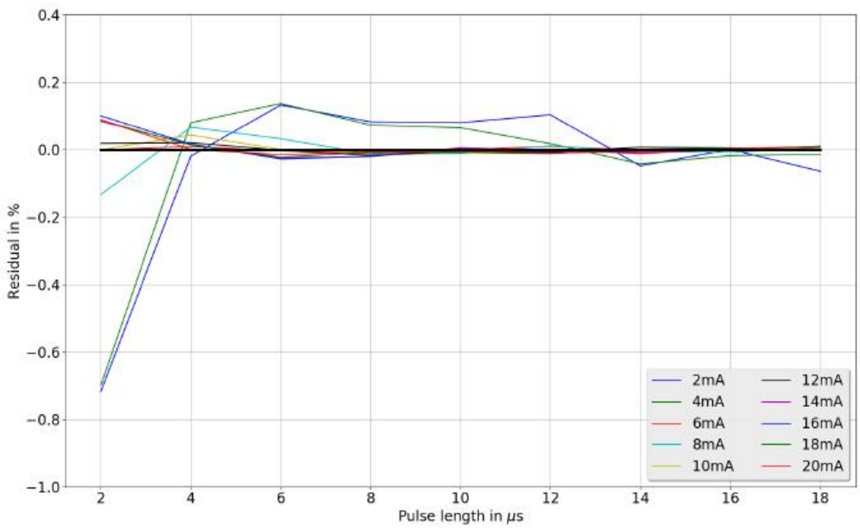

Figure 6.2.: *Residuals of measurement on the dependence of the diode current on the pulse length at a constant input current from the linear fit.*

The residuals show that there are deviations up to 1% from the line fit at short pulse lengths, especially at the first point at $2\,\mu$s. However, for pulses at least 4μs long all data points lie within 0.2% of the linear fit which is a strong indication that diode current rises linearly with the pulse length. Since the pulse length that is used in the field is $5\,\mu$s, the measurement technique should work well.

A similar analysis for constant pulse length yields the results shown in Figure 6.3 and Figure 6.4.

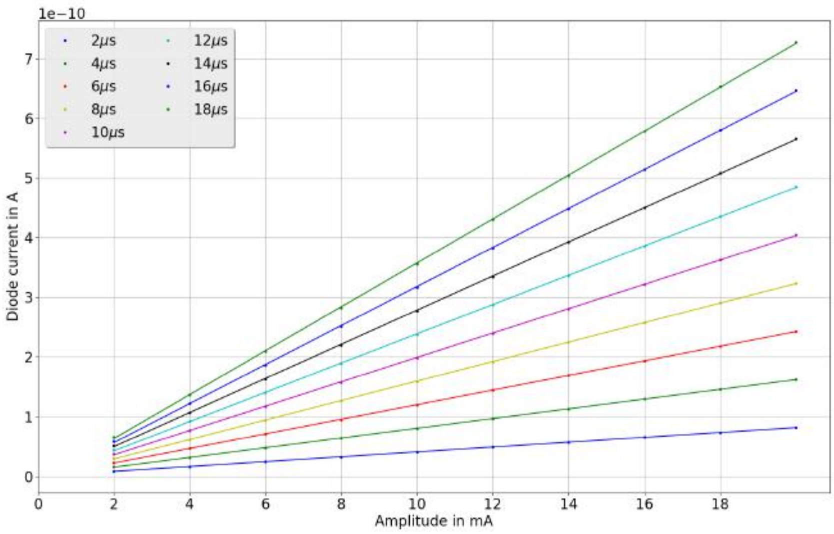

Figure 6.3.: *Full measurement on the dependence of the diode current on the input current at a constant pulse length. The measurements again agree with the line fits very well.*

The data in Figure 6.3 shows again a high agreement with the linear fit which can also be seen at the residuals shown in Figure 6.4.

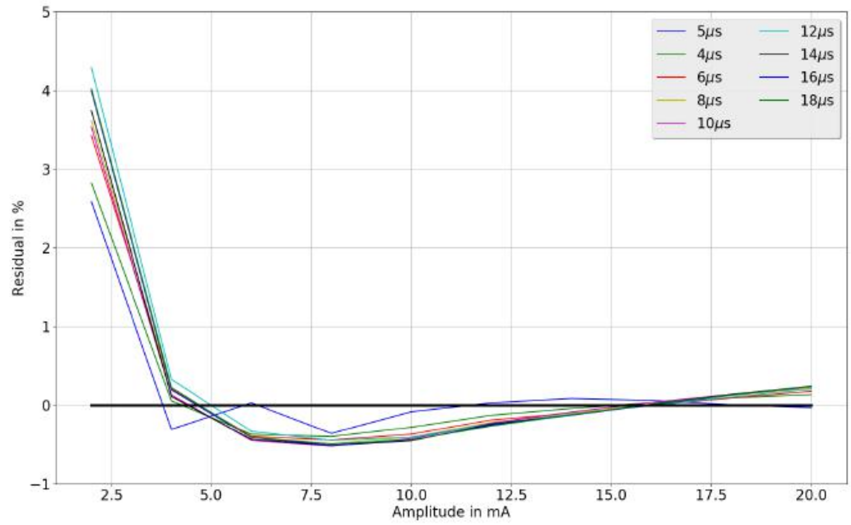

Figure 6.4.: *Residuals of measurement on the dependence of the diode current on the input current from at a constant pulse length the linear fit.*

Here, the deviations are larger than those measured, in dependence of the pulse length. This is expected since the response curve of the LEDs is not perfectly linear as can be seen in Figure A.1. Nevertheless the deviation from the linear fit is always lower than 4.5% and at currents higher than 4 mA it is always less than 1%.

From this it is possible to conclude that the linear dependence of the diode current on both the input current and the pulse length can be seen which shows that the technique of using a pulsed source to mimic a DC signal in the diode, as presented in section 5.1, behaves as expected.

6.2. PMT data

The PMT is used to get single pulse information such as the pulse length and the pulse integral. In order to get this information, a clean separation between the baseline and the pulse itself is needed. To do this, three different methods of pulse identification were tested as described in the following section.

6.2.1. Pulse classification

The first algorithm consists of a threshold value which, due to the negative signal, is given by $\frac{1}{2}$ of the minimum value in the pulse. Anything lower than this value is counted as part of the signal. This algorithm has the advantage of having a very good time complexity of $O(n)$ where n is the length of the array. However, it does not give any information about how many points are in the rising or falling edge of the pulse which can lead to fluctuations in the identified pulse length as can be seen in Figure B.1. It also leads to an underestimation of the pulse length at small amplitudes since the influence of the slope on the rising and falling edge are much higher compared to higher input currents.

The second algorithm included is based on a running average. For each data point the average value of the data is calculated for the region of the surrounding ± 25 points. From these averages it searches for the point with the highest change in the mean. These points are going to be where the pulse begins and ends. This algorithm is run separately on each pulse resulting in a total time-complexity of $O(l \cdot n \log(n))$ where l gives the number of pulses and n the number of points in a pulse. Since this algorithm is looking for the point on the edges of the pulse, it does give some information about the edges, though not in a way that allows easy identification of edge points.

As the final algorithm in this comparison, the unsupervised learning algorithm DB_scan as set up in the python scikit-learn library [11] is used. This algorithm creates an epsilon environment of given size around each point and checks if there are a specified number of neighbouring points in its surroundings. Any point that satisfies these conditions will be included into one cluster. The advantage of this algorithm is that both the baseline and the signal are included into individual clusters and that any point on one of the edges is classified as outlier. For this reason it is easy to get information about the rising and falling edges since those points are now separated from the rest. However, it is also possible that points of the signal get classified as outliers or that the cluster breaks at some point in the signal or carries on into the baseline. Apart from that, with a time-complexity of $O(l \cdot n^2)$, it has the longest run times of the presented algorithms which makes the application difficult.

A comparison of the performance of all three methods can be seen in Figure 6.5.

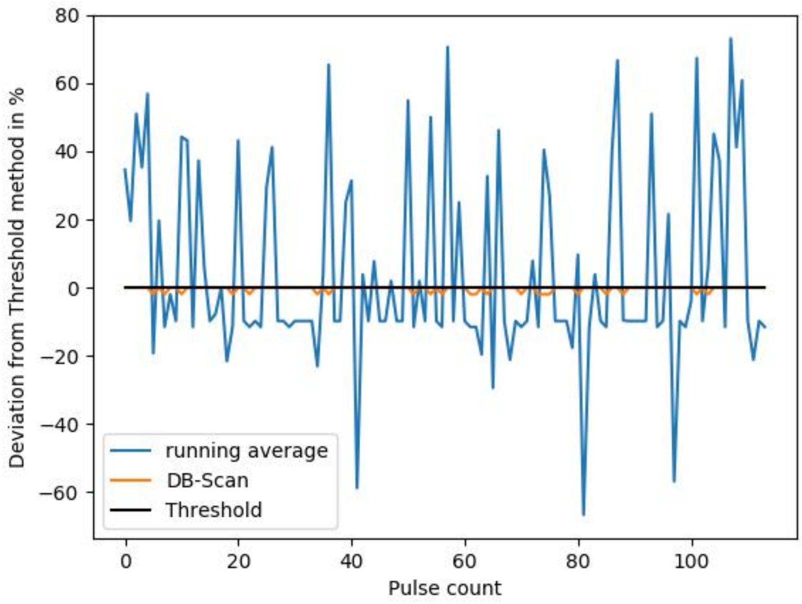

Figure 6.5.: *This figure shows a comparison between the pulse length found by the three algorithms normalized to the result of the threshold method.*

Figure 6.5 shows the pulse length specified by each algorithm in comparison to the threshold method. The threshold method is chosen as the baseline since it will return a number that is close to the exact value, it is computationally efficient and is unlikely to fail completely.

As can be seen the threshold and db-Scan agree very well with a maximum deviation of about 2%, while the running average shows huge fluctuations with more than 60% deviation. Since the other two methods agree it is highly unlikely that the value the running average returns is correct. This might be due to errors in the implementation of the specific method, or it being not well suited to the task.
The highest deviation between the DB-Scan and the threshold method is about 2% which corresponds to about two points of the signal. This small performance improvement does not justify the several times longer run times of the DB-Scan algorithm. For this reason the threshold method is used in the following analysis for PMT data.

After the pulses are identified, the pulse length and pulse integrals are extracted. The pulse length is calculated by multiplying the sampling rate by the number of points detected as part of the signal. The integral is calculated by simply summing all points in the signal after subtracting the baseline. For further analysis, the mean and standard deviation of each measurement set is calculated and used representative for that set of measurements.

6.3. Baseline measurement

For the baseline measurement, the script *measurement_bl* is used. It is based on the calibration measurement script with the only difference being that the LEDs are turned off using the command option

```
python runFlasher.py -n 0 --no-leds
```

The measurement was repeated 31 times.

6.3.1. Diode

The result of all the baseline measurements combined is shown in Figure 6.6.

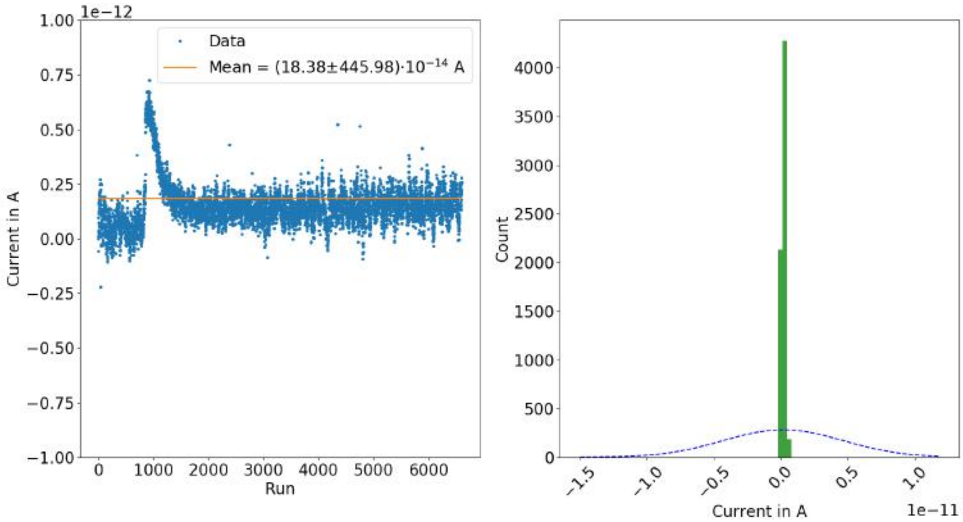

Figure 6.6.: *This figure shows the full baseline measurement. At the start of the measurement there is a jump and fall off in the baseline current visible, which can not be explained. This also leads to problems in performing a Gaussian fit on the data as can be seen in the plot on the right*

In the first 1500 points, Figure 6.6 shows a jump followed by a slow fall of in the baseline current before it stabilizes at around $20 \cdot 10^{-14}$ A. This jump can not be due to single flashes since each point corresponds to half a second of integration time and about 1 s between measurements. Neither is opening the dark box or light leaking a likely explanation since this would result in a much higher signal (The diode signal with an opened box is about 42 nA.). In addition it would not decay over a time of several minutes (approximately 1000 points correspond to about 30 min) but rather give a rectangular drop-off in the signal. To discover the full explanation of this behavior further investigation is needed. The right part of Figure 6.7 shows that the points far on the outside of the typical measurement have skewed the measured mean toward lower values. Since this behavior can not be described the first ∼1800, points which corresponds to 6 script iterations are removed from the baseline calculation. The results of the baseline measurement after this treatment can be seen in Figure 6.7

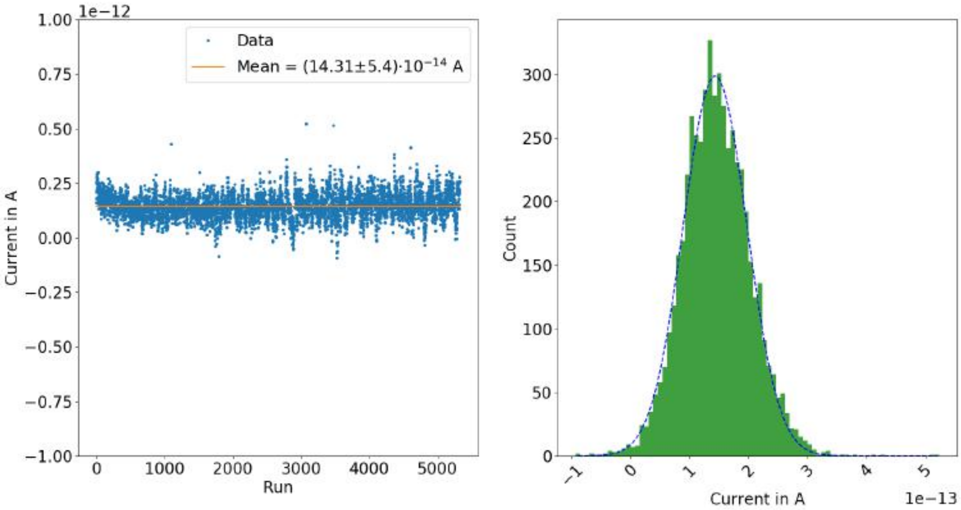

Figure 6.7.: *This figure shows the baseline measurement after the two first measurements are removed. The distribution on the right hand side can now be described as Gaussian.*

It can be seen here that the distribution of points after cuts is much closer to the Gaussian fit shown in blue on the right side of Figure 6.7. From this, in the following measurements a baseline diode current of

$$I_{base,diode} = (14.3 \pm 5.4) \cdot 10^{-14} A \tag{6.1}$$

will be assumed.

6.3.2. PMT

During the above measurements, the baseline of the PMT is recorded as well. The result of this is shown in Figure 6.8.

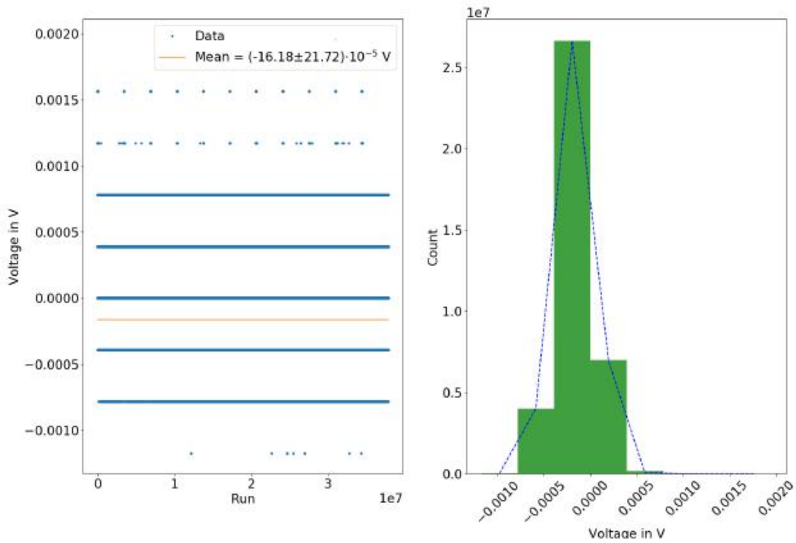

Figure 6.8.: *This figure shows the baseline measurement using the PMT. The measurements are highly discrete.*

Figure 6.8 shows a highly discrete measurement steps on these low currents. This is due to the 8-Bit data of the Picoscope. This can be seen looking at the data, as the steps starting from 0 are clearly seen in Table 6.1.

Table 6.1.: *Comparison of the discrete measurements with an 8-Bit signal.*

line	measured voltage in V	0.1*line/256
0	0	0
1	0.00039067	0.0003906
2	0.00078134	0.0007813
3	0.00117201	0.0011719
4	0.00156269	0.0015625

It is clear that the accuracy of the measurement is limited by this discretization. However, from a Gaussian function fitted to the distribution of measurements, as shown on the right side of Figure 6.8, a baseline of

$$U_{\mathrm{dark,PMT}} = -0.162 \pm 0.195\,\mathrm{mV} \tag{6.2}$$

can be extracted. The error of this is taken as half of the step size.

6.4. Calibration measurement

To run the calibration measurement, the script *measurement* is used. At a pulse length of $5\,\mu$s it runs through the given range of flasher LED input currents. In the measurements shown, it runs from 0.1 mA to 10 mA in 0.1 mA steps. To flash at a controlled rate, the flasher is triggered with an external function generator which sends signals at a rate of 100 Hz. The PMT captures the first 2000 pulses while on the diode 200 measurements with an integration time of 0.5 s are made. During the evaluation of all $2 \cdot 10^6$ PMT pulses there were no pulses where a trigger was sent that was not followed by a signal from the LED. However, there has not yet been a measurement specifically made to verify this absolutely.

6.4.1. Diode

For every flasher setting, a distribution of the data points is created from which the mean and standard deviation are taken as representative for the whole measurement. An example measurement at 5 μs and 2.7 mA set can be seen in Figure 6.9.

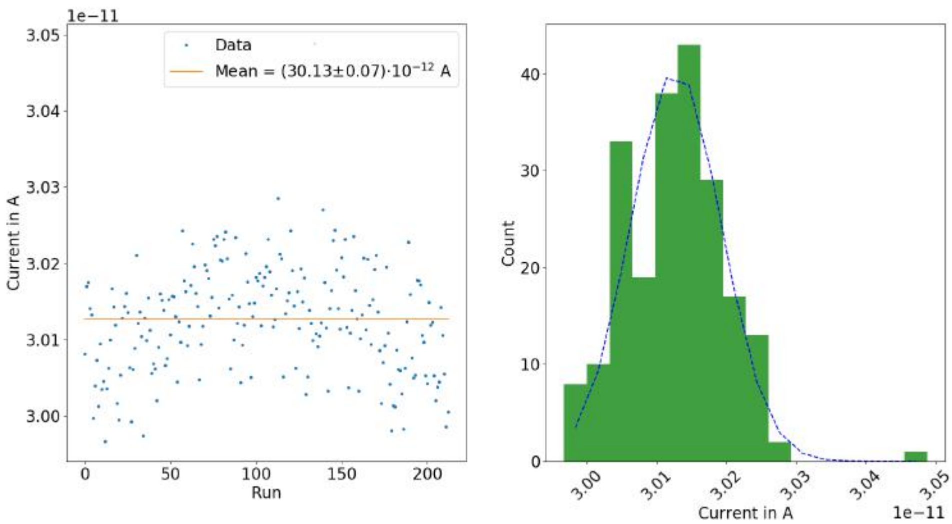

Figure 6.9.: *Example diode measurement at 5μs and 2.7 mA. The left side shows the evolution of the current from run to run. The right side shows a histogram of the data with a Gaussian function fitted to it with the center at $30.13 \cdot 10^{-12}$ A and a width of $0.99 \cdot 10^{-14}$ A with the error of the mean given in the plot.*

For the calibration measurement the current on the LEDs is increased which, if the LED response to current is linear, should lead to a proportional increase of the diode current. To show this the mean diode current as a function of the input current is plotted in Figure 6.10.

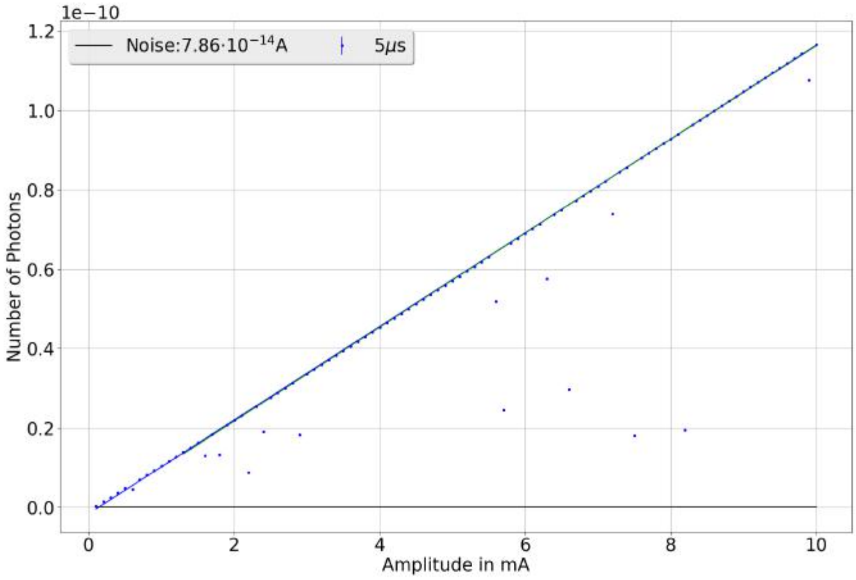

Figure 6.10.: Linear fits on the means with errors given by $\frac{\sigma}{\sqrt{n}}$. One fit is going through all data points while the second starts at 1.5 mA. One can see a clear linear trend. Some points are far away from the linear fit however only below the line. Close to the 0 line the noise is plotted.

In Figure 6.10 there are several points that do not agree with the line fit. All of these point are at a lower mean current than the linear fit would suggest. The reason for this behavior can be seen in Figure 6.11 which shows one of these problematic measurements at 4.5 mA input current.

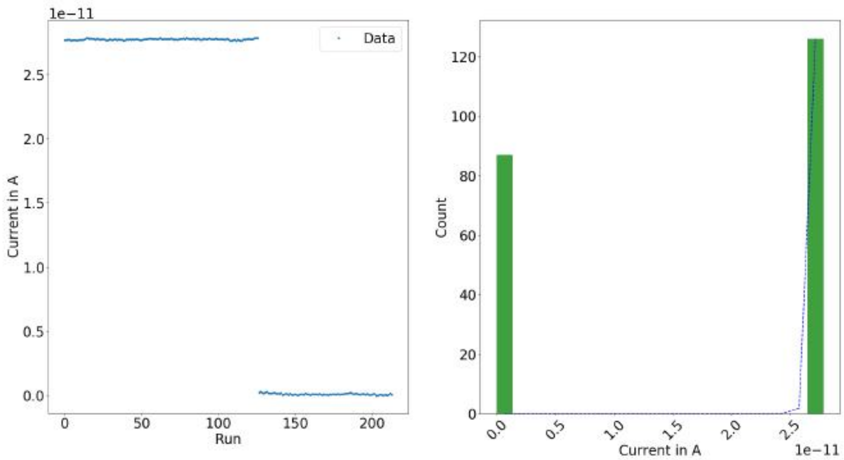

Figure 6.11.: Problematic measurement at 4.5 mA. Compared to Figure 6.9 Diode current drops about half way through the measurement to the level of the baseline (see Figure 6.7).

Similar things happen at all the other measurements that do not agree with the linear fit. The most likely reason for this behavior is some internal problem of the flasherboard. It is also possible that this is a desynchronization of the command scripts, though this was designed against as the measurement script states that the flasher should go on flashing until the picoamperemeter has finished its measurement.

The signal height on the lower end in Figure 6.11 is on the level of the baseline (compare with section 9.1). This allows us to assume that the flasher is turned off during this time so that these points can be cut from the data. To do this a threshold of 70% of the maximum current in each measurement setting is introduced. Anything below this threshold is cut out. Doing this with all data points leads to Figure 6.12.

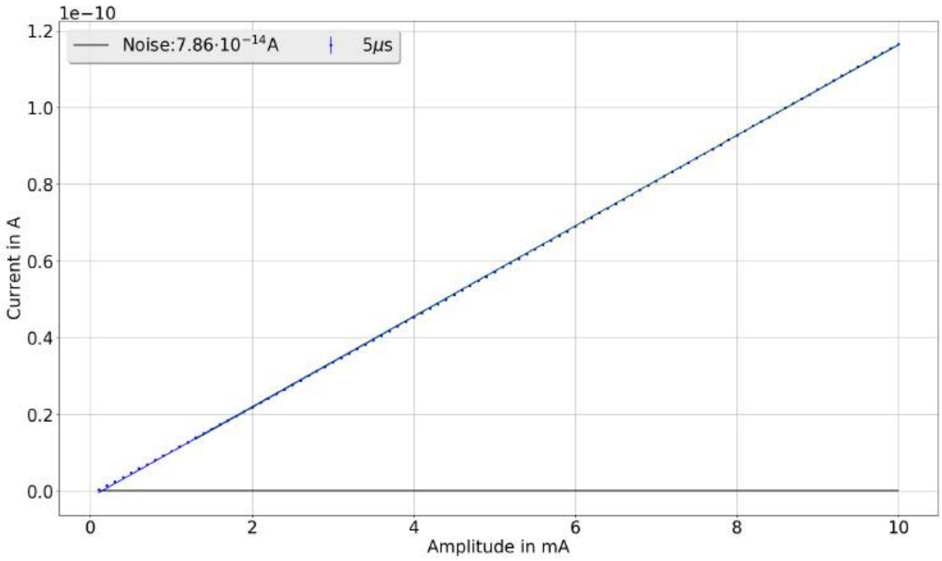

Figure 6.12.: *Same figure as Figure 6.10 with a cut if the data in each point is drops below 70% of the maximum value. Errors are given by* $\frac{\sigma}{\sqrt{n}}$.

In Figure 6.12 the linear dependence of the diode current on the input amplitude can be seen clearly. The residuals from this fit are shown in Figure 6.13.

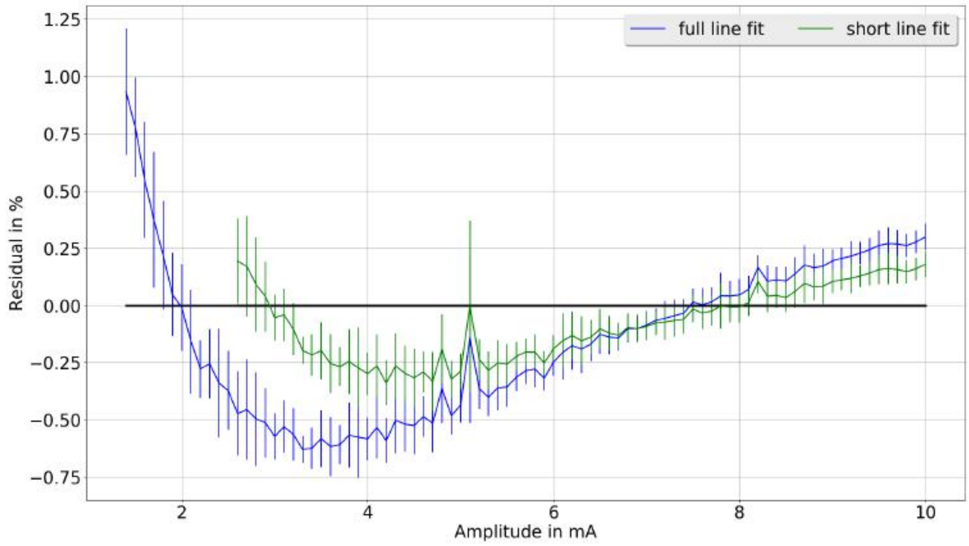

Figure 6.13.: *Residuals between the line fit and the data points shown in Figure 6.12. Errors are given by the error of the mean with a picoamperemeter error of 0.4% added in quadrature. For the green data points the linear fit starts at 2.5 mA On the second shorter line fit the deviation is <0.5% and the line fit is within the error margin of all points.*

At input currents higher than 2 mA the deviation from the linear fit is smaller than 1% while at lower currents the fluctuations are much larger. For this reason a second line fit starting at 2.3 mA is performed to model the stable data more accurately. The errors are given by the standard deviation together with a 0.4% error on the picoamperemeter measurement, as specified in the manual, summed in quadrature.

The slopes of the two fits are listed in Table 6.2 with the error given by the fit algorithm.

Table 6.2.: *Comparison of the fitted slopes for the three measurements*

Slope 1 in A/mA	Slope 2 in A/mA
$(1.1790 \pm 0.0085) \cdot 10^{-11}$	$(1.1838 \pm 0.0069) \cdot 10^{-11}$

From the slope a calibration constant can be deduced that satisfies the equation

$$N_{\gamma,\mathrm{Sphere}} = C_{\mathrm{calib}} \cdot \frac{I_{\mathrm{input}}[\mathrm{mA}]}{[\mathrm{mA}]} \cdot \frac{t_{\mathrm{pulse\ length}}[\mu\mathrm{s}]}{[\mu\mathrm{s}]}. \tag{6.3}$$

This is possible since it was shown in subsection 6.1.1 that the response of the diode with respect to the input current and pulse length is almost perfectly linear. Since the measurements here were taken at a pulse length of 5 μs the calibration constant is given by

$$C_{\mathrm{calib}} = \mathrm{Slope} \cdot \frac{C_{\mathrm{conv}}}{5} = (3.789 \pm 0.002) \cdot 10^{8} \tag{6.4}$$

Therefore, the number of photons emitted can be written as

$$N_{\gamma,\text{sphere}} = (3.789 \pm 0.002) \cdot 10^8 \cdot \frac{I_\text{input}}{[\text{mA}]} \frac{t_\text{pulse length}}{[\mu\text{s}]} \tag{6.5}$$

As can be seen in Figure 6.13 the linear fit does not perfectly agree with the measured data. Therefore, this number can only be used to get an estimate on the number of produced photons.

6.4.2. PMT

The analysis of the PMT data is split into several steps. First the signal has to be detected. This is done using the threshold method as described in subsection 6.2.1. After this the pulse length and the pulse integral are calculated.

In order to get the pulse length the known sampling rate of the Picoscope is multiplied by the number of points that are classified as being part of the signal. The integral is similarly calculated by adding up all current values of the data points in the signal region.

For every flasher setting 2000 samples are taken and the mean and standard deviation are calculated. Figure 6.14 shows the dependence of the pulse length on the input current. Since the pulse length should not depend on the pulse amplitude one would expect a constant pulse length.

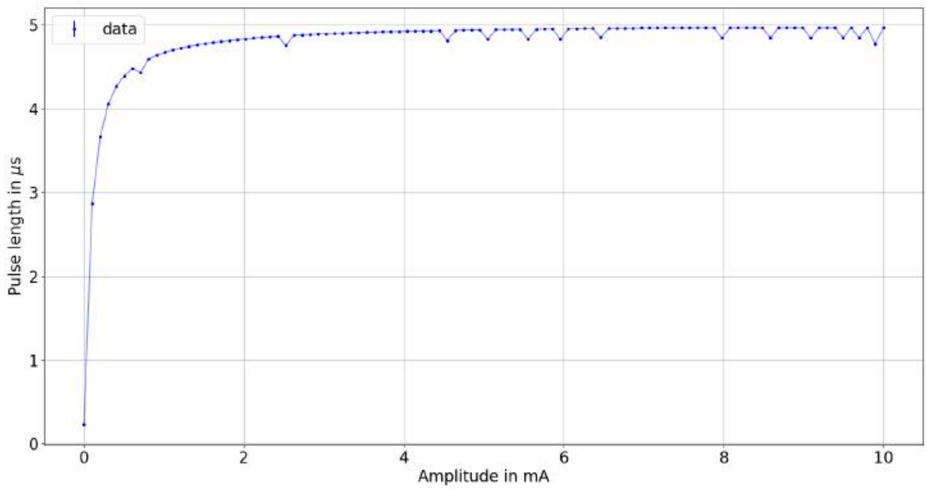

Figure 6.14.: *This figure shows the pulse length in microseconds depending on the input current of the flasher LEDs. There is a steep rise in the pulse length that is approaching the expected value of 5 μs.*

Figure 6.14 shows that there is a rise in the pulse length that is, apart from a few outliers, the same for all three measurements. A possible explanation, besides it being a feature of the hardware, for this shape could be the threshold classification method. Especially at low signal heights, the noise in the signal might be high enough to push points so low as to not be classified as part of the pulse. This effect becomes more unlikely at higher amplitudes which leads to an increasing mean pulse length. Here, effects such as classifying points in the rising and falling edge as part of the signal might change the pulse length.

Apart from the pulse length the pulse integral is recorded as well. As with the photodiode a linear dependence of the integral on the input current is expected. A plot of the integral can be seen in Figure 6.15

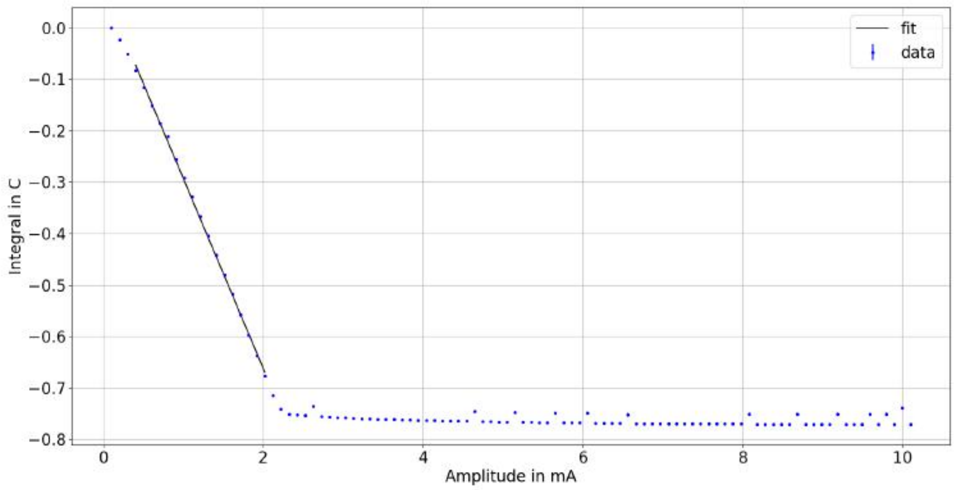

Figure 6.15.: *This figure shows the pulse integral depending on the input current of the flasher LEDs. In between 0.4 mA and 1.9 mA a linear fit is plotted. At higher input currents the measurement saturates.*

In contrast to what would be expected from the pulse length plot in Figure 9.7 the integral looks very linear between 0.4 mA ans 2 mA. Above 2 mA the Picoscope runs into its range limit of 50 mV and therefore no higher integrals can be recorded. This can easily be addressed in the future by using a smaller PMT mask. In the linear region the line fit agrees reasonably well with the linear fit which can also be seen in Figure 6.16.

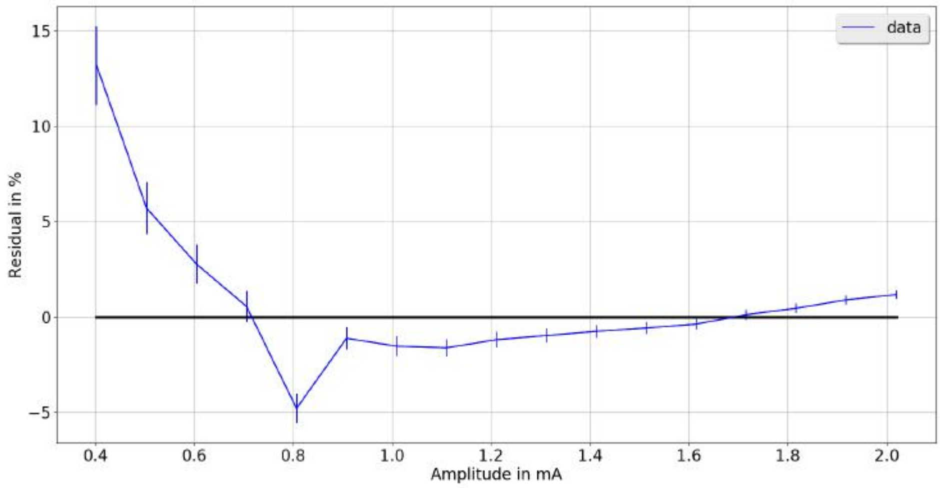

Figure 6.16.: *This figure shows the residuals from the line fit of the pulse integral depending on the input current of the flasher LEDs .*

Figure 6.16 shows high deviations from the line at low currents that decrease with increasing pulse amplitude. Above 0.5 mA all measurements are within 5% of the linear fit. The deviation at very low currents could be due to non-linearity of the LEDs at these low input currents since a similar behavior can be observed on the diode as well.

When looking at the pulse area stability shown in Figure 6.17 the area variability looks, apart from one spike at 0.8 mA, nearly constant across the whole measurement range.

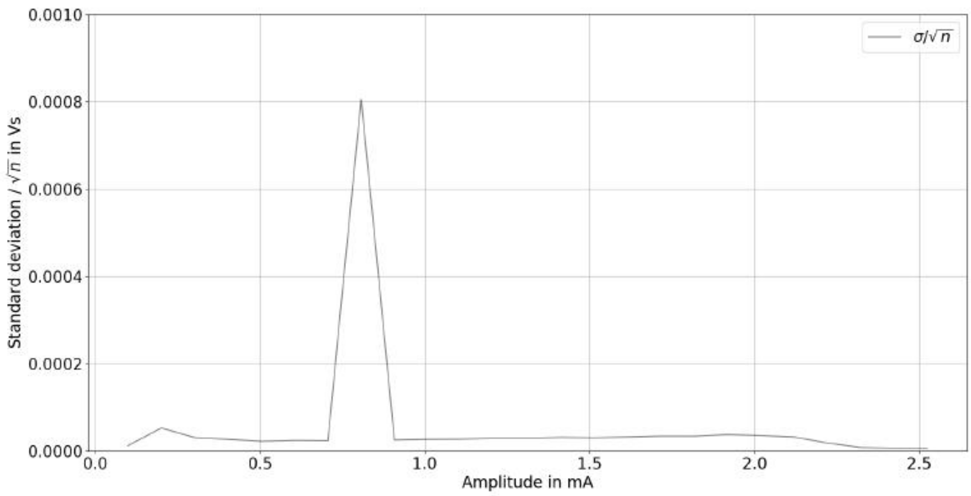

Figure 6.17.: *This figure shows the standard deviation in each measurement set. Apart from one spike at 0.8 mA the standard deviation is almost constant at $\frac{\sigma}{\sqrt{n}} < 0.0001$ Vs. The spike can be seen in both the standard deviation and the residuals shown in Figure 6.16 and is most likely caused by corrupted data.*

From Figure 6.17 the standard deviation can be estimated to be σ ~0.0045 Vs which corresponds to a pulse to pulse fluctuation of < 1% at an integral of -0.1 Vs but decreases linearly as the integral increases linearly. Unfortunately, the PMT measurement saturates at ~2 mA so that no information about the pulse area variability above this current can be given with absolute certainty at this time. However, the pulse area variability for input currents >1 mA is ~1% and since this value is expected to decrease for higher input currents this number will be used as an upper bound of the uncertainty for input currents >2 mA.

The spike at 0.8 mA occurs both in the standard deviation and in the residual plot. This spike can be traced back to a problem in the measurement which is shown in Figure C.1.

6.4.3. 1 Hz measurement

In order to show that the 100 Hz calibration is scalable to the 1 Hz pulse rate which is used for the actual FD calibration, several measurements with pulse amplitudes 2.6 mA, 2.7 mA, 2.8 mA, 2.9 mA and 3.0 mA are made at a flashing rate of 1 Hz and compared to the 100 Hz measurement between 2.0 mA to 3.0 mA. The result of this comparison is shown in Figure 6.18.

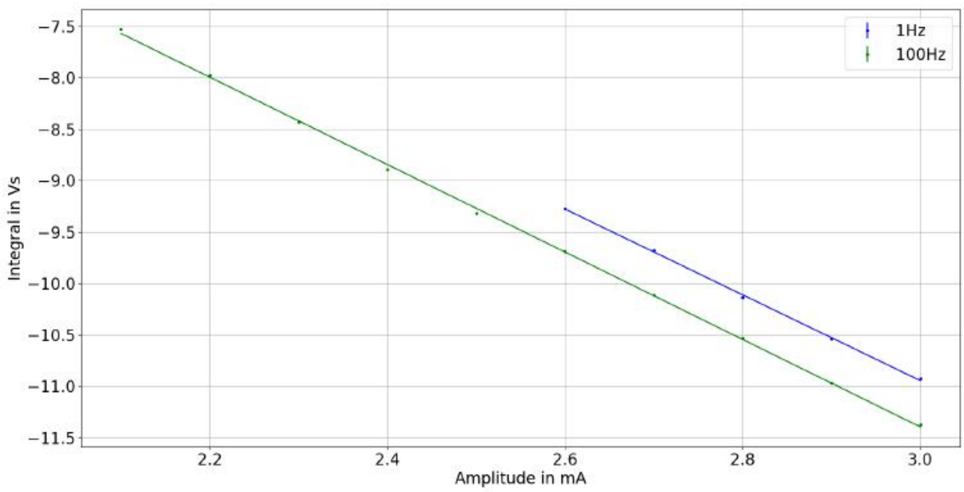

Figure 6.18.: *This figure shows the mean integrals for measurements at 100 Hz and 1 Hz .*

Figure 6.18 shows that there is a offset between the measurement at 1 Hz and 100 Hz, while the slopes of the two lines are listed in Table 6.3.

Table 6.3.: *Comparison of the fitted slopes for the measurement*

Slope 100 Hz in Vs/mA	Slope 1 Hz in Vs/mA
-4.25 ± 0.03	-4.16 ± 0.07

There is a 2% deviation between the two slopes, however their errors overlap. This might be due to there being too few measurement points and is expected to decrease if more measurements are added. To convert the measurement at 100 Hz, a linear function as well as a constant was fit to the ratio of the 100 Hz and 1 Hz measurement was performed. The result of this is shown in Figure 6.19.

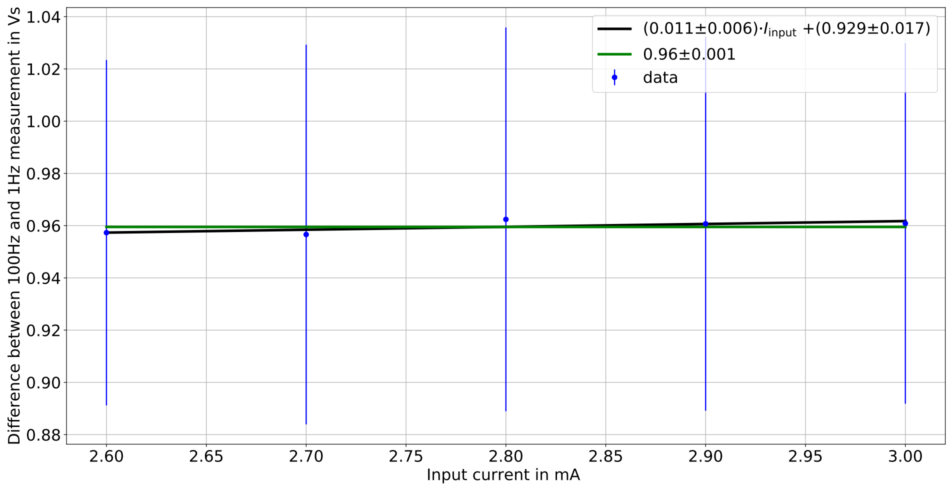

Figure 6.19.: *Difference between the 100 Hz and 1 Hz measurement with a linear and a constant fit.*

Judging from the data shown in Figure 6.19 there is no reason to assume that the offset is not constant. Therefore the conversion between 100 Hz and 1 Hz can be done by multiplying the measured mean extracted by the constant fit at 100 Hz by

$$C_{100\to 1} = 0.959 \pm 0.001 \tag{6.6}$$

where the error is the returned error of the mean. This corresponds to a decrease by

$$(4.1 \pm 0.1)\% \tag{6.7}$$

of the measurement value at 100 Hz. Since only very few data points have been taken so far, this can only assumed to be true in the input current range from 2.6 mA to 3 mA. For the absolute calibration on other ranges more data points need to be taken.

7. Uncertainties

In the following chapter an account of the calculation of the uncertainties in the absolute calibration is given.

7.1. Geometric Uncertainties

The geometric uncertainties which arise from the set up were discussed in subsection 5.2.2. To review, they involve the uncertainty in the distance between the lambertian surface and the diode Δd, the manufacturer quoted uncertainty in the size of the diode Δa, as well as the uncertainty in the port size of the sphere Δr.

The geometric uncertainties represent the main contribution of the set up to the total error of the calibration. They are the same for all measurements as long as there is no change in the distance between the measurements.

Their calculation is done by applying the following formula

$$\sigma_i = \Delta i \cdot \frac{\partial \Phi_{\text{diode}}}{\partial i} \tag{7.1}$$

to the conversion Equation 3.14 with $i \in \{d, a, r\}$. From these individual uncertainties the total geometric uncertainty is given by

$$\sigma_{\text{geo}} = \sqrt{\sigma_{\text{d}}^2 + \sigma_{\text{a}}^2 + \sigma_{\text{r}}^2} \tag{7.2}$$

The errors estimated for the geometric uncertainty are listed in Table 7.1

Table 7.1.: *Geometric uncertainty*

Uncertainty	Value
Δd	2mm
Δa	10 μm
Δr	0.2mm

7.2. Instrumentation uncertainty

The instrumentation uncertainty describes the uncertainty in the measurement due to the measurement uncertainties of the picoamperemeter and the Picoscope.

The uncertainty of the picoamperemeter $\Delta I_{\text{picoamp}}$ is given by the number quoted in the manual [8] while for the Picoscope $\Delta U_{\text{Picoscope}}$ half of the step size in the discrete measurements is taken (see subsection 6.3.2). Since the error of the picoamperemeter directly translates to an uncertainty in the calibration and the error in the Picoscope doe not, the larger error on the Picoscope does not have a significant impact on the measurement. It is necessary to have this value as small as possible. The values of the instrumentation uncertainty are listed in Table 7.2

Table 7.2.: *Instrumentation uncertainty*

Uncertainty	Value
$\Delta I_{\text{picoamp}}$	0.4%
$\Delta U_{\text{Picoscope}}$	0.195 mV

7.3. Diode baseline uncertainty

The baseline of the diode measurement can be seen as an indicator of how quiet the measurement environment is. When the baseline current of $(1.43 \pm 0.54) \cdot 10^{-13}$ is compared to a typical signal, such as the 2.7 mA measurement, a signal to noise ratio of

$$\frac{I_{2.7\,\text{mA}}}{I_{\text{baseline}}} = \frac{30.13 \cdot 10^{-12}\,A}{14.31 \cdot 10^{-14}\,A} = 210 \tag{7.3}$$

is found. Since the absolute calibration is done after subtracting the baseline the uncertainty in the baseline has a direct influence on the calibration result. The baseline uncertainty is given in Table 7.3

Table 7.3.: *Diode baseline uncertainty*

Uncertainty	Value
$\Delta I_{\text{baseline}}$	$7 \cdot 10^{-14}$ A

7.4. Diode DC current uncertainty

The DC current uncertainty involves both the accuracy of the measuring method and the spread of the measurements taken. The accuracy of the method is estimated in subsection 6.1.1 to follow linearity within 1%. The spread of the measurement is usually around $1 \cdot 10^{-13} A$ which corresponds to about 0.3% of the measurement. This contribution is however considerably decreased since the error of the mean is used for further calculations.

Table 7.4.: *Diode DC current uncertainty*

Uncertainty	Value
$\Delta I_{\text{linearity}}$	1%
ΔI_{spread}	$1 \cdot 10^{-13}$ A

7.5. Pulse to pulse area uniformity

The pulse area uniformity gives an estimation on how big the variation between the recorded area of the individual recorded pulses are. This is important to know since the calibration is done for single pulses. The pulse area uniformity measurement has several points of uncertainty. The pulse selection using the threshold method creates uncertainties in both the pulse length and the pulse integral. Figure B.1 leads to the estimation that the rising and falling edge together take up about 2% of the pulse. Since the cut is made at 50% of the maximum signal the pulse this leads to an underestimation of the pulse length of ∼1%. Since there is a small slope in the edges this leads to changing estimations for the pulse integral. This influence become smaller at higher input currents as the change in the slope will decrease. Since the variation of the integral of the pulses for all flasher settings have been observed to be on the order of 0.3% taking the full uncertainty estimation of each pulse's ∼1% seems reasonable.

Table 7.5.: *Pulse to pulse area variability*

Uncertainty	Value
$\Delta \int$	1%

7.6. 100 Hz to 1 Hz conversion uncertainty

As described in subsection 6.4.3 a conversion from 100 Hz measurements to 1 Hz measurements is needed. This is necessary since the XY-Scanner will be operating at a flashing frequency of 1 Hz. The conversion is seen to be a constant factor of 0.959 ± 0.001. The error of this is the resulting accuracy of a constant fit on the data, which includes the errors of each of the taken measurements.

Table 7.6.: *100 Hz to 1 Hz conversion*

Uncertainty	Value
ΔC_{conv}	0.1%

7.7. Efficiency uncertainty

The uncertainty in the efficiency describes the error in the conversion of the measured diode current to a number of photons hitting the diode. The biggest contribution to this is the uncertainty of the calibration given by Hamamatsu [6] which is 2%. Other than that there is the uncertainty of the web-plot-digitizer [14] and the interpolation function created by Mathematica for both the calibration and the LED spectrum. This is estimated to be about 0.1%.

Table 7.7.: *Efficiency uncertainty*

Uncertainty	Value
Δ calib	2%
Δ digitization	0.1%

7.8. Unknown error budget

The unknown error budget is estimated to be about 3% of the total measurement. This involves errors such as temperature dependence or misalignment of the diode and sphere and any other errors that might occur in the measurement that have not been treated before in chapter 7.

8. Absolute calibration

After all the previous considerations a preliminary absolute calibration can be calculated. The input current chosen for this is 2.7 mA as this is the value the KIT team used in the field on the observatory's fluorescence telescopes.

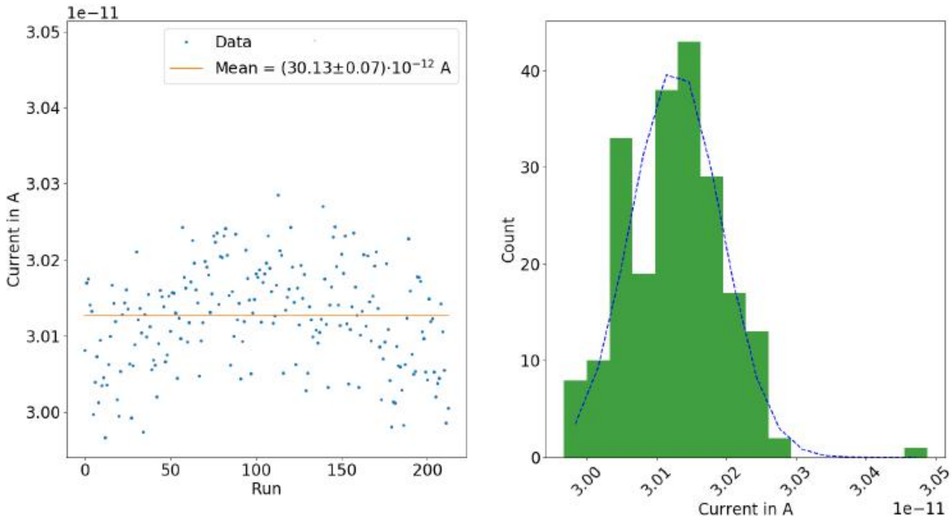

Figure 8.1.: *Measurements at 2.7 mA and the distribution of points on the right side.*

The measurements shown in Figure 8.1 are used to calculate the number of photons leaving the sphere. The calibration Equation 3.14 is then used to convert this mean current into a photon count. The distance from the diode to the sphere is set to (20.0±1.31) cm and the efficiency is taken from section 3.1. This leads to a photon count per flash of

$$N_{\gamma,\mathrm{Sphere},100\,\mathrm{Hz}} = (4.9883 \pm 0.1622) \cdot 10^9 \tag{8.1}$$

Finally to get a photon count at a flashing rate of 1 Hz the number has to be multiplied by the previously calculated conversion factor of (0.959±0.001), which leads to the final calibration number of

$$N_{\gamma,\mathrm{Sphere},1\,\mathrm{Hz}} = (4.7872 \pm 0.2) \cdot 10^9. \tag{8.2}$$

All errors involved in this calculation are listed below.

Table 8.1.: *Measurement uncertainties at 2.7 mA LED current and 5μs pulse length*

Measurement:	Uncertainty	Uncertainty in Photons	Uncertainty in %
Picoamperemeter	0.4%	1.93×10^{7}	0.40
Measurement	7.0×10^{-14} A	1.12×10^{7}	0.24
Baseline	5.4×10^{-14} A	8.64×10^{6}	0.013
Efficiency	$2.9428 \times 10^{-3} \frac{A}{W}$	9.64×10^{7}	2.08
100→1	0.1%	1.21×10^{7}	0.25
Geometry:			
Δr	0.2 mm	9.64×10^{6}	0.21
Δd	2 mm	9.50×10^{7}	2.05
Δa	10 μm	8.64×10^{5}	0.019
	Total	1.38×10^{8}	2.98
	3% unaccounted	2.00×10^{8}	4.32

9. KIT sphere and upgrade

Between the 22nd and 25th of August 2019, a team from KIT brought their sphere to Wuppertal to obtain an absolute calibration measurement and to perform a hardware upgrade on the Wuppertal sphere, which would allow us to change the LED input current in steps of 0.1 mA.
This visit was critical as the KIT sphere has already been used to perform a telescope calibration and therefore an absolute calibration of their source would allow for an end-to-end absolute calibration of the observatory. In the following an absolute calibration for the Karlsruhe sphere and a comparison of the old and new hardware are presented. For this purpose, the following measurements were made

1. Baseline measurement
2. Calibration measurement:
   3 times from 0.1 mA to 5 mA at a pulse length of 5 μs on the new hardware
3. Calibration measurement:
   From 1 mA to 20 mA at a pulse length of 5 μs on the old hardware

Other than the sphere used in Wuppertal, the KIT sphere comes with a 2 in port reducer which is coated with highly reflective paint on the inside. This is assumed to move the lambertian surface to the plane of the port reducer. This also changes the distance to the diode to

$$d_{\text{port reducer}} = 18.46 \pm 1.2\,\text{mm}. \tag{9.1}$$

The change in the accuracy is due to the much better defined position of the lambertian surface.

9.1. Baseline measurement

A new baseline measurement is done using the *measurement_bl* script. This was necessary since the KIT flasherboard does not have its LEDs desoldered and they might contribute to the baseline noise. The measurement was repeated 11 times.

9.1.1. Diode

The result of all the measurements combined is shown in Figure 9.1.

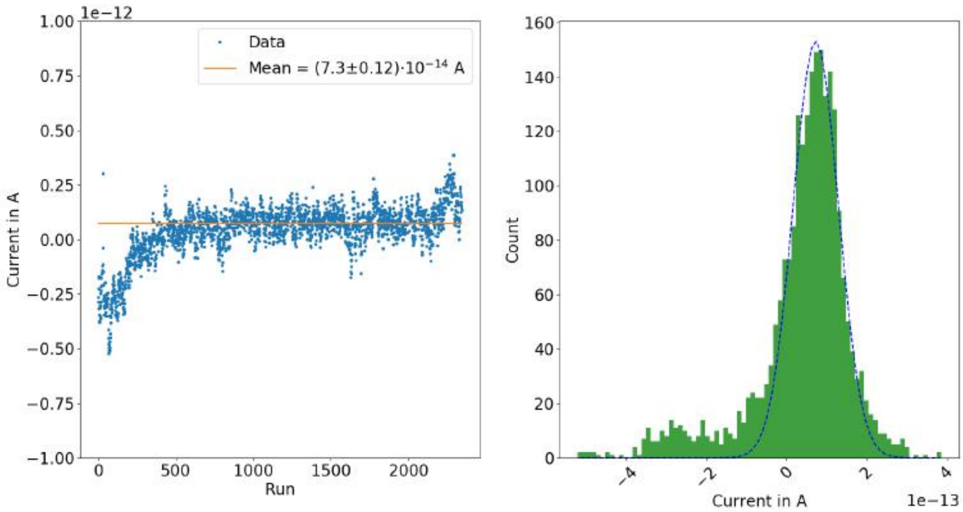

Figure 9.1.: *This figure shows the full baseline measurement. At the start of the measurement there is a change in the baseline current.*

In the first 500 points Figure 9.1 shows a change in the baseline current. This change could be due to electric components heating up until a steady state is reached. The right part of Figure 9.2 shows the distribution of the points which is skewed toward lower currents. Since this behavior can not be described the first two out of the eleven measurements are cut out which corresponds to about 400 points in Figure 9.1. The result of this can be seen in Figure 9.2.

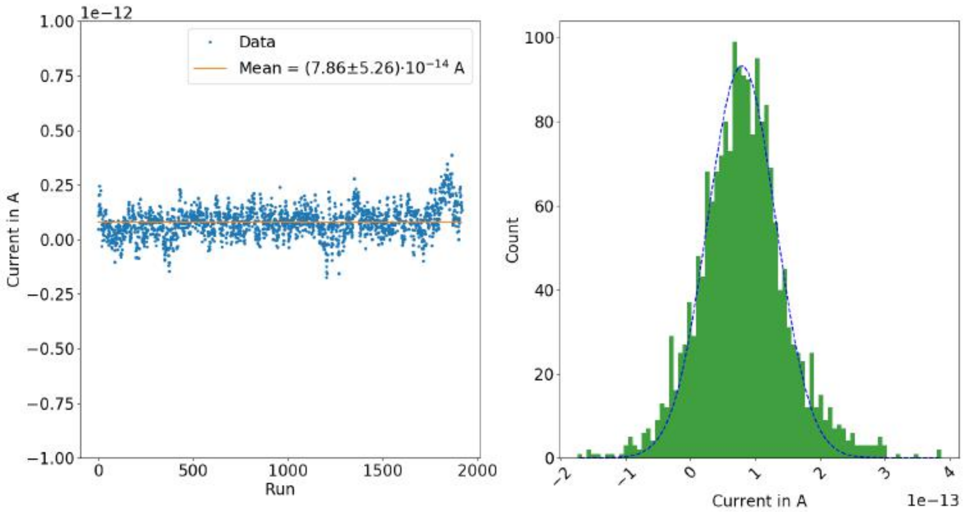

Figure 9.2.: *This figure shows the baseline measurement with the two first measurements removed. The distribution on the right hand side can now be described by a Gaussian fit function.*

The resulting distribution of point is much closer to a Gaussian distribution which is fitted in blue on the right side of Figure 9.2. For the following measurements a baseline diode current of

$$I_{base,Diode} = 7.86 \pm 0.11 \cdot 10^{-14} A \tag{9.2}$$

is going to be assumed.

9.1.2. PMT

In the same measurement, the baseline for the PMT is recorded as well. The result of this is shown in Figure 9.3.

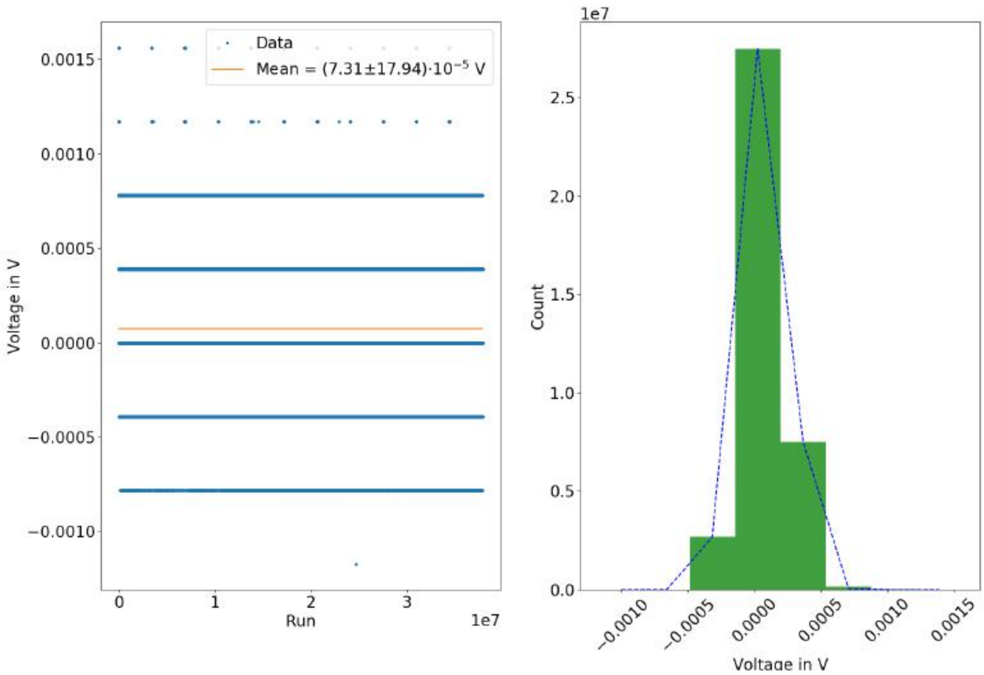

Figure 9.3.: *This figure shows the baseline measurement using the PMT. The measurements are highly discrete.*

Figure 9.3 shows again a highly discrete measurement similar to what could be seen in Figure 6.8. This is due to an 8-Bit discretization of the measurement range.
From a Gaussian function fit to the distribution of the points, as shown on the right side of Figure 9.3, a baseline of

$$U_{\mathrm{dark,PMT}} = 0.731 \pm 0.401 \mathrm{mV} \tag{9.3}$$

can be extracted. The error on this is given by $\frac{\sigma}{\sqrt{n}}$ with n the number of sample points.

9.2. Calibration measurement

The calibration measurement is done with the *measurement* script. For the new hardware it runs from 0.1 mA to 5 mA and for the old hardware from 1 mA to 20 mA. The flasher is triggered with an external function generator which sends signals at a rate of 100 Hz. The PMT captures the first 2000 pulses while the picoamperemeter takes 200 measurements of the diode current with an integration time of 0.5 s.

9.2.1. New Hardware

For the new hardware the calibration measurement in between 0.1 mA and 5 mA is done three times.

Diode

Running the same analysis as described in subsection 6.4.1 results in the calibration curve shown in Figure 9.4.

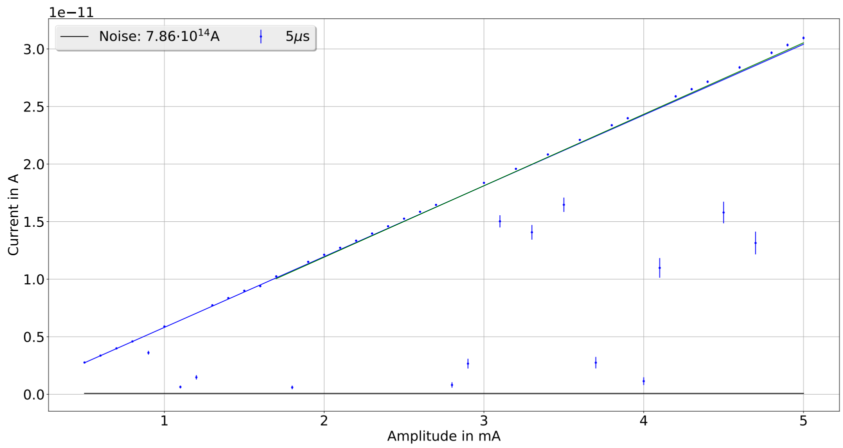

Figure 9.4.: *Linear fits on the means of Measurement 1 with error given by $\frac{\sigma}{\sqrt{n}}$. One fit goes through all data points while the second starts at 15 mA. One can see a clear linear trend. Some points are far away from the linear fit, though only below the line.*

Comparing Figure 9.4 to the results seen in Wuppertal (Figure 6.10) similar problems can be seen. For this reason the same cut at 70% of the maximum current measured is performed which leads to the results shown in Figure 9.5.

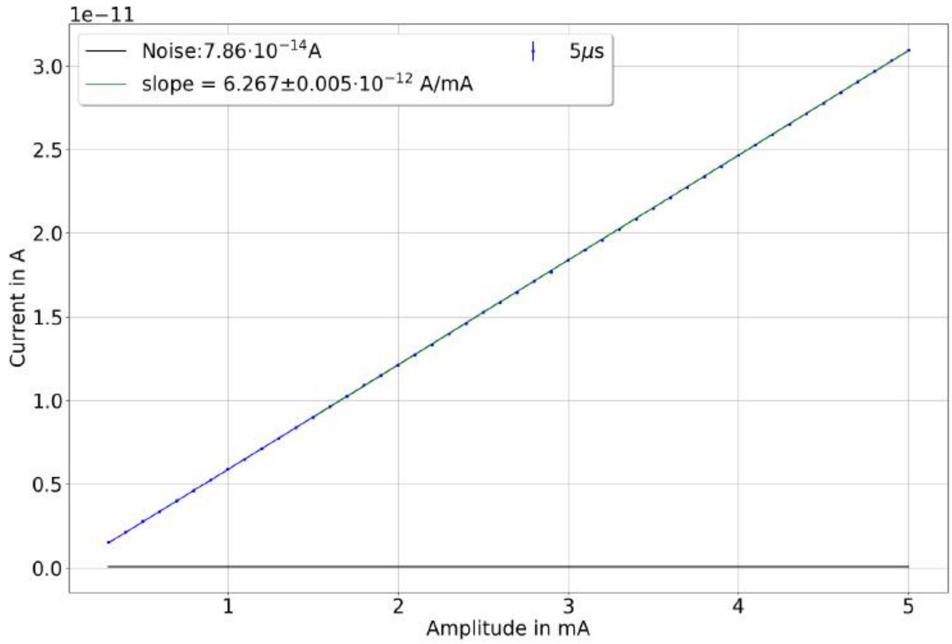

Figure 9.5.: *Same figure as Figure 9.4 with a cut if the data in each point is drops below 70% of the maximum value. Errors are given by $\frac{\sigma}{\sqrt{n}}$.*

In Figure 9.5 the linear dependence of the diode current on the input amplitude can clearly be seen. The residuals from this fit are shown in Figure 9.6.

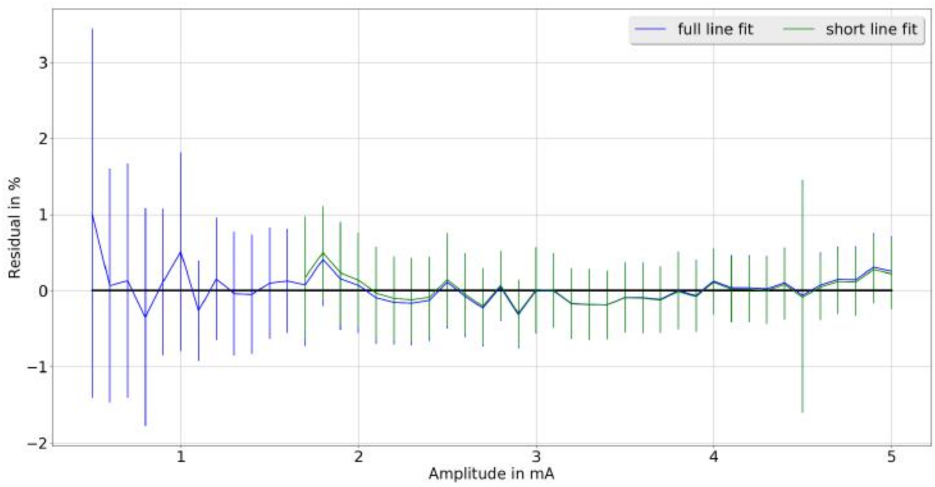

Figure 9.6.: *Residuals between the line fit and the data points shown in Figure 9.5. Errors are given by $\frac{\sigma}{\sqrt{n}}$ with a 0.4% error of the picoamperemeter. Above 2 mA the deviation is <0.5%*

At input currents higher than 1 mA the deviation rarely exceeds 0.5% while at lower currents the fluctuations are much larger. This can also be seen on the other two measurements. For this reason a second line fit starting at 1.5 mA is performed to model the stable data more accurately.

The same analysis is performed for the other two measurement runs. The result of these runs can be found in the Appendix Figures B.2 to B.5.

The slope of the two fits for all three measurements can be found in the following Table 9.1.

Table 9.1.: *Comparison of the fitted slopes for the three measurements and the $\frac{\chi_2^2}{ndf}$ of the second line fit.*

Slope 1 in A/mA	Slope 2 in A/mA	$\frac{\chi_2^2}{ndf}$
$(6.277 \pm 0.002) \cdot 10^{-12}$	$(6.257 \pm 0.005) \cdot 10^{-12}$	0.105
$(6.242 \pm 0.003) \cdot 10^{-12}$	$(6.246 \pm 0.007) \cdot 10^{-12}$	0.083
$(6.248 \pm 0.003) \cdot 10^{-12}$	$(6.254 \pm 0.005) \cdot 10^{-12}$	0.121

The data in Table 9.1 shows the agreement of the slopes is very good and that the error margins on all three of the measurements overlap. The low $\frac{\chi_2^2}{\text{ndf}}$ could be due to an overestimation of the error on the picoamperemeter measurement which are likely systematic. All the constant errors for example on the distance and alignment are not taken into account here as they are shared between measurements. These errors are accounted for later in the uncertainty calculation.

From the slope a calibration constant can be deduced that satisfies the equation

$$N_{\gamma,\text{Sphere}} = C_{\text{calib}} \cdot I_{\text{input}}[\text{mA}] \cdot t_{\text{pulse length}}[\mu\text{s}] \tag{9.4}$$

Since the measurements here were made at a pulse length of 5 μs the calibration constant is given by

$$C_{\text{calib}} = \text{Slope} \cdot \frac{C_{\text{conv}}}{5} = (3.2186 \pm 0.0016) \cdot 10^8 \tag{9.5}$$

9.2.2. PMT

As before the analysis of the PMT data is split into several steps. First the signal has to be detected. This is done using the threshold method as described in subsection 6.2.1. After this is done the pulse length and the pulse integral are calculated.

For every flasher setting 2000 samples are taken and the mean and standard deviation of all pulses in each set are calculated. Figure 9.7 shows the dependence of the pulse length on the input current. Since the pulse length does not depend on the pulse amplitude one would expect a constant pulse length.

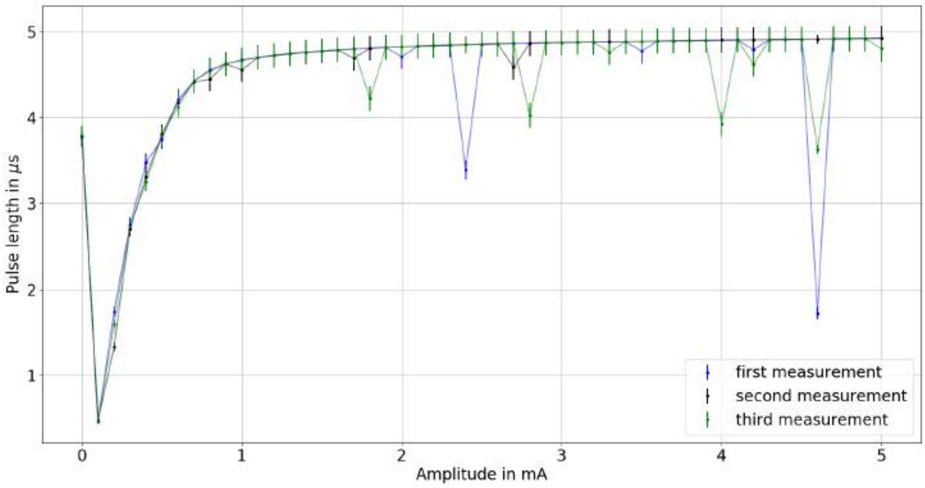

Figure 9.7.: *This figure shows the pulse length in microseconds depending on the input current of the flasher LEDs. There is a steep rise in the pulse length that is approaching the expected value of 5 µs. The jump at 0 mA arises since it is not possible to pass 0 mA to the flasher and it returns to the default settings.*

Figure 9.7 shows that there is a rise in the pulse length that is, apart from some few outliers, the same for all three measurements. Similar to what was seen in Figure 6.14 the pulse length are much smaller at input currents smaller than 1 mA when compared to higher input currents. A possible explanation for this shape could be an underestimation due to the threshold classification method at low currents as was explained in section 6.2. Or it being a specific feature of the flasherboard. To see if this is the case, more measurements are needed.

Apart from the pulse length the pulse integral is recorded as well. As with the photodiode, a linear dependence of the integral on the input current is expected. A plot of the integral can be seen in Figure 9.8

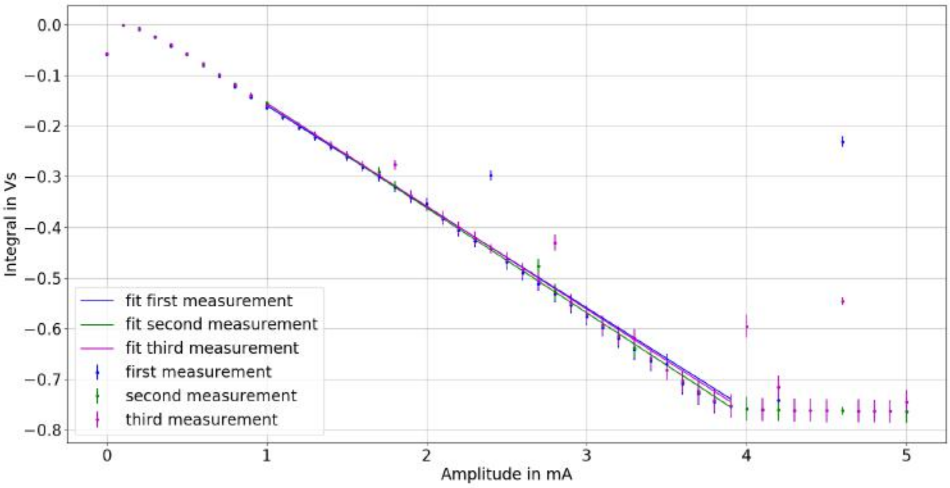

Figure 9.8.: *This figure shows the pulse integral depending on the input current of the flasher LEDs for all three measurements. In between 1 mA and 3.9 mA a linear fit is plotted*

Similar to what could be seen in section 6.2, in contrast to what would be expected from the pules length plot in Figure 9.7, the integral looks very linear down to 0.1 mA. Above 4 mA the Picoscope runs into the range limit,and therefore no higher integrals are recorded. The high agreement in the center with the linearity can also be seen in Figure 9.9. There are several outliers that appear both in the linearity and the residual plot. The cause can not be explained with certainty though it is likely to have similar problems as can be seen in Figure C.1.

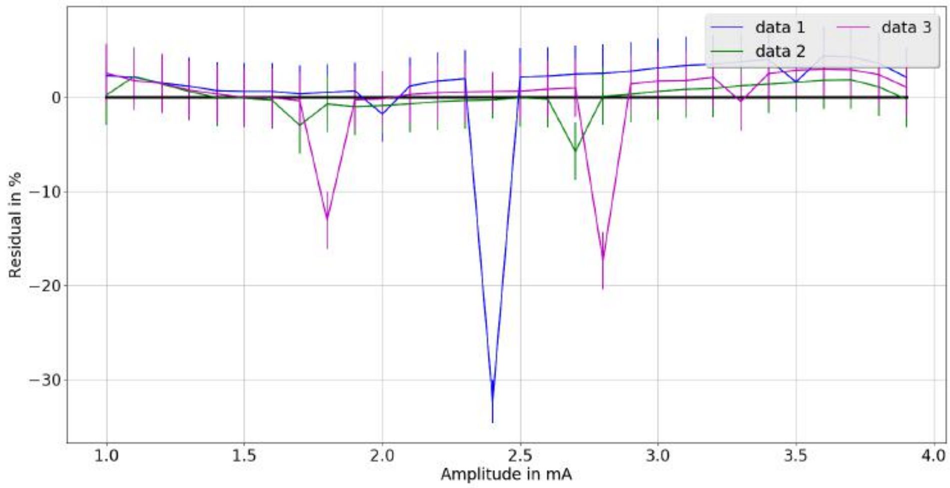

Figure 9.9.: *This figure shows the residuals from the line fit of the pulse integral depending on the input current of the flasher LEDs for all three measurements.*

Figure 9.9 also shows high deviations from the line at low currents. It both over and under estimates the values. To explain this further investigation is needed. At input currents greater than 4 mA the deviation is due to the saturation of the measurement

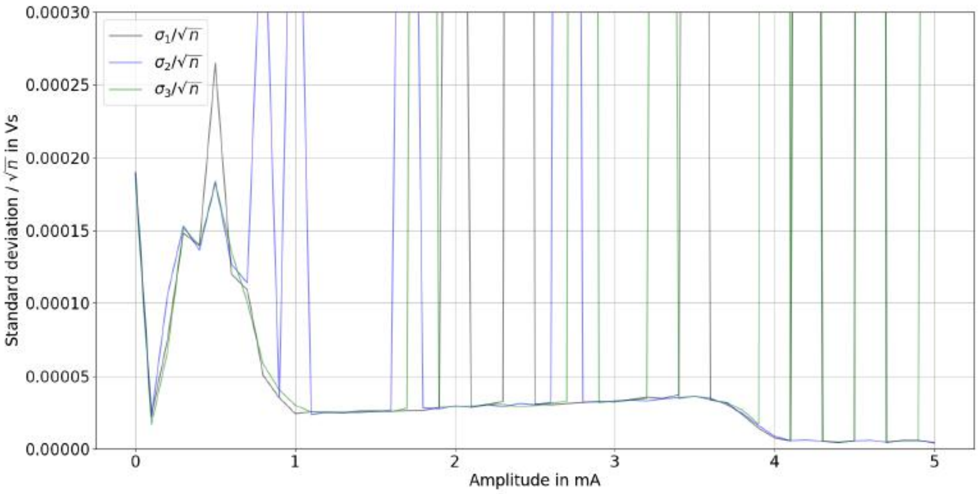

Figure 9.10.: *This figure shows the standard deviation in each measurement set. Apart from some spikes the standard deviation is almost constant at* $\frac{\sigma}{\sqrt{n}} < 0.0005$ *Vs, which corresponds to less than 0.03% of the mean.*

When looking at the pulse area stability shown in Figure 9.10 there is a peak that ends at around 1 mA. This is expected since it is in the unstable region of input currents below 1 mA. At higher input currents the area variability rises, apart from some spikes, slowly until it falls of once the measurement saturates. Overall it stays below 0.00005 Vs, which corresponds to less than 0.03% of the mean.

9.2.3. Absolute calibration

After all the previous considerations an absolute calibration can be calculated. This is done again for 2.7 mA input current .

For this purpose all three of the measurements at 2.7 mA are combined and the mean of that distribution, which is shown in Figure 9.11 ,is used to calculate the number of photons leaving the sphere.

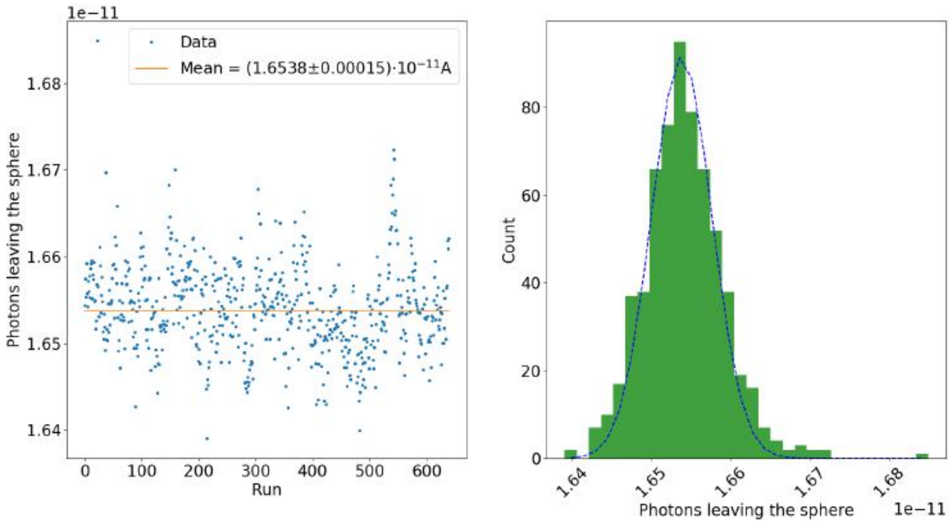

Figure 9.11.: *Measurements at 2.7 mA and the distribution of points on the right side.*

In this case the conversion is already folded into the distribution of the points. The total number of points leaving the sphere at 2.7 mA is

$$N_{\gamma,\text{Sphere}} = (2.248 \pm 0.085) \cdot 10^9 \tag{9.6}$$

To convert this to a flashing rate of 1 Hz the same considerations as in section 6.2 can be made which leads to a photon count of

$$N_{\gamma,\text{Sphere}} = (2.157 \pm 0.083) \cdot 10^9 \tag{9.7}$$

The errors are listed below in Table 9.2.

Table 9.2.: *Measurement uncertainties at 2.7 mA LED current and 5µs pulse length*

Measurement:	Uncertainty	Uncertainty in Photons	Uncertainty in %
Picoamperemeter	0.4%	8.99×10^6	0.40
Measurement	1.5×10^{-15} A	2.88×10^6	0.134
Baseline	1.1×10^{-15} A	2.11×10^5	0.098
Efficiency	$2.9428 \times 10^{-3} \frac{\text{A}}{\text{W}}$	4.5×10^7	2.08
100→1	0.1%	5.62×10^6	0.25
Geometry:			
Δr	0.2 mm	4.49×10^6	0.21
Δd	2 mm	2.41×10^7	1.12
Δa	10 µm	2.93×10^5	0.014
	Total	5.23×10^7	2.43
	3% unaccounted	8.54×10^7	3.86

9.3. Old Hardware

A similar analysis as presented in subsection 9.2.1 is performed on the old Hardware. Since only steps of 1 mA are available now the range for this measurement has to be changed to go from 1 mA to 20 mA. Again, the *measurement* script was used with the adopted range.

9.3.1. Diode

After performing the cut as described in section 9.2.1 the calibration measurement shown in Figure 9.12.

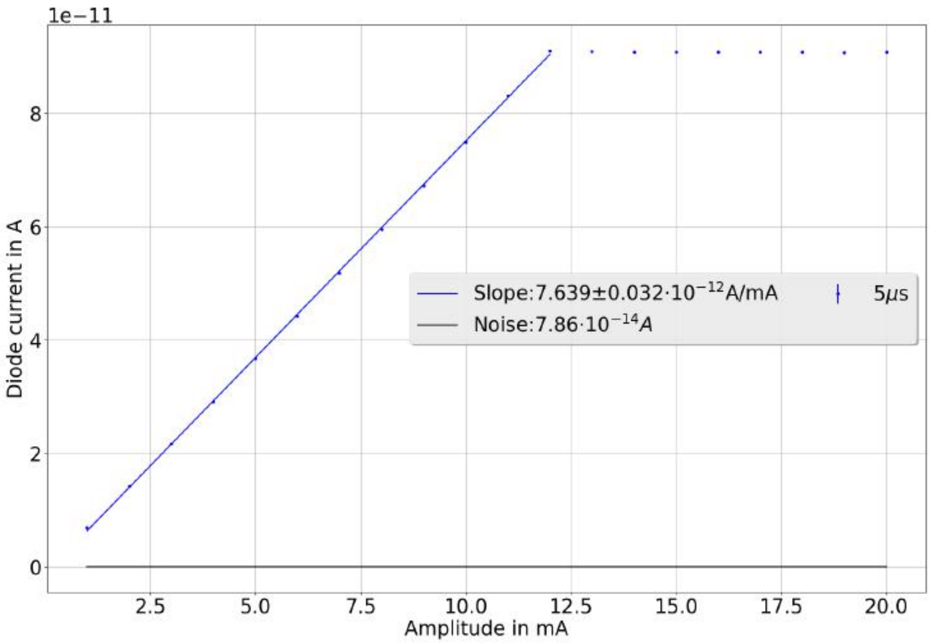

Figure 9.12.: *Calibration measurement with old Hardware. At 12 mA the connection with the flasher was lost which resulted in it flashing continuously at the last updated setting*

The cut off at 12 mA is due to a connection loss with the flasher. Since the settings could not be updated, the flasher kept flashing at the last setting passed to it before the connection was lost.

From 3 mA to 12 mA a linear fit has been made with a slope of $(7.639 \pm 0.032) \cdot 10^{-12}\,\frac{\text{A}}{\text{mA}}$ which is 15% different from the slope measured with the new hardware. This could be explained both by the change in hardware and the different measurement range which goes up to higher input amplitudes. The residuals are shown in Figure 9.13.

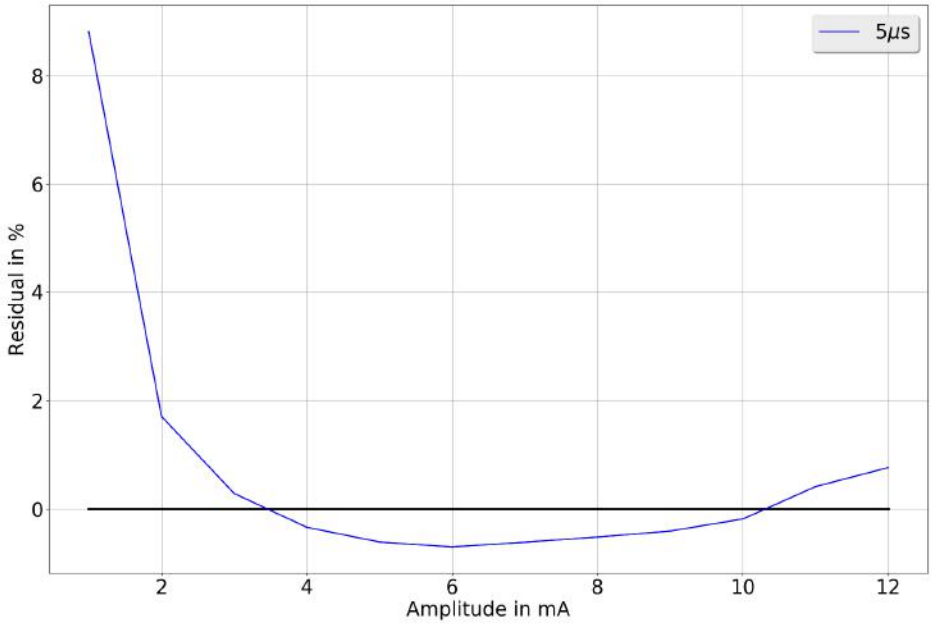

Figure 9.13.: *Residuals of the calibration measurement shown in Figure 9.12 with old Hardware.*

Figure 9.13 shows that at low and very high currents the linear fit under estimates the diode current. Between 4 mA and 10 mA it overestimates the current. This leads to a significantly different fit when only points up to 5 mA are measured, which could also explain the difference in the slopes between new and old hardware.

9.3.2. PMT

Similar to the diode, the PMT data, taken with the old Hardware, is analyzed as described as before in subsection 9.2.2. First, looking at the pulse length we find the behavior shown in Figure 9.14.

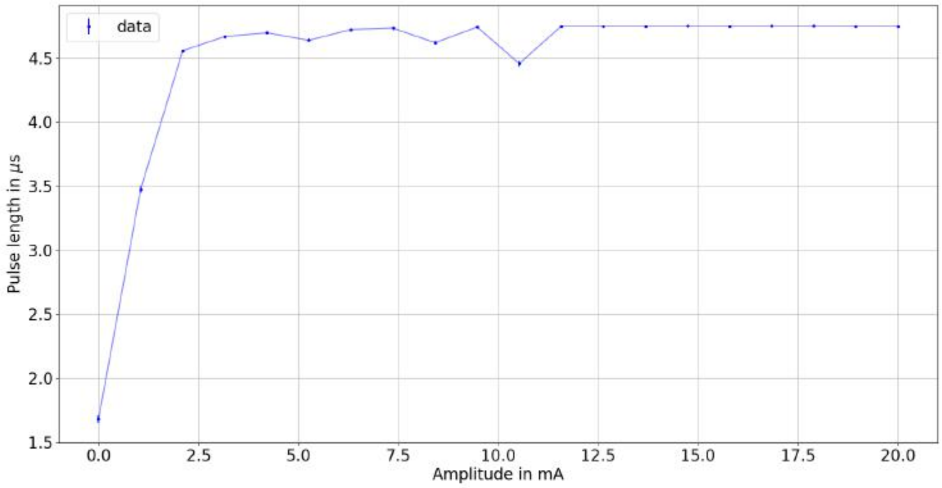

Figure 9.14.: *This figure shows the pulse length in microseconds depending on the input current of the flasher LEDs measured on the old hardware. There is a steep rise in the pulse length that is approaching the expected value of 5 μs similar to what can be seen on the new hardware in Figure 9.7*

Again, there is a cut off at 12 mA due to the connection loss. Similar to what has been seen on the new hardware there steep rise in the pulse length at low input currents. On the new hardware the pulse length stabilizes at around 1 mA. On the old hardware this happens at 2 mA. This time however it takes longer until the pulse length saturates.

The pulse integral can be seen in the following Figure 9.15.

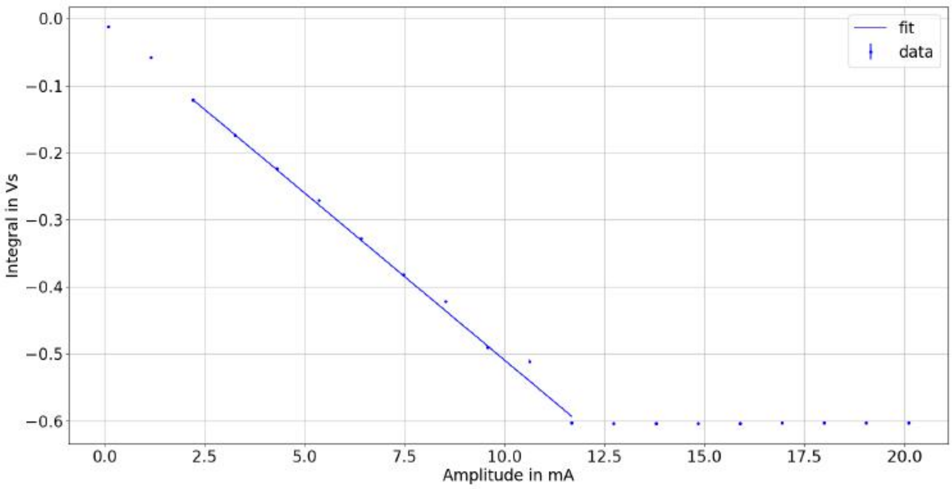

Figure 9.15.: *Pulse integral of the calibration measurement on the old Hardware.*

From Figure 9.15 one can see that the integral before the cut off follows a line reasonably well. This can also be seen in Figure 9.16 which shows the residuals from the linear fit.

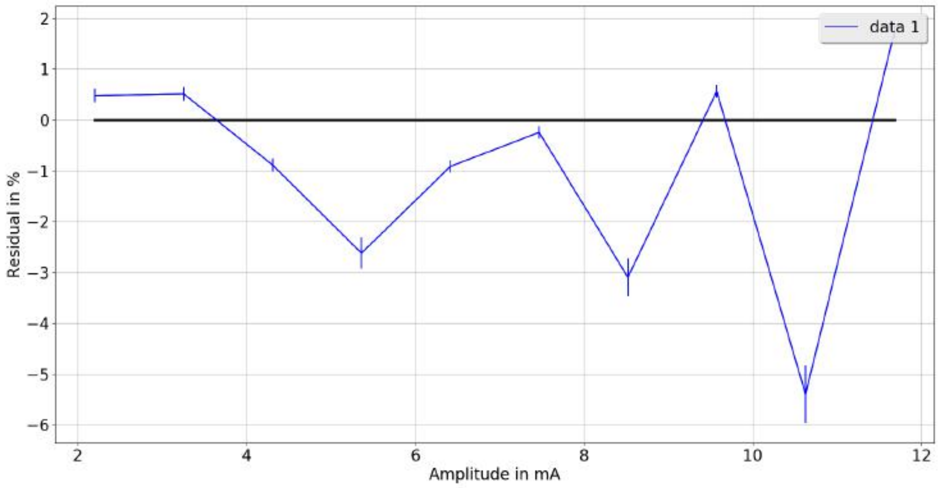

Figure 9.16.: *Residual of the pulse integral of the calibration measurement shown in Figure 9.15 on the old hardware.*

The deviations from the line are a lot higher than with the diode measurement in Figure 9.13. However, when compared to the residuals on the pulse integrals taken with the new hardware in Figure 9.9 this appears to be reasonable. The standard deviation on the measurements is shown in Figure 9.17.

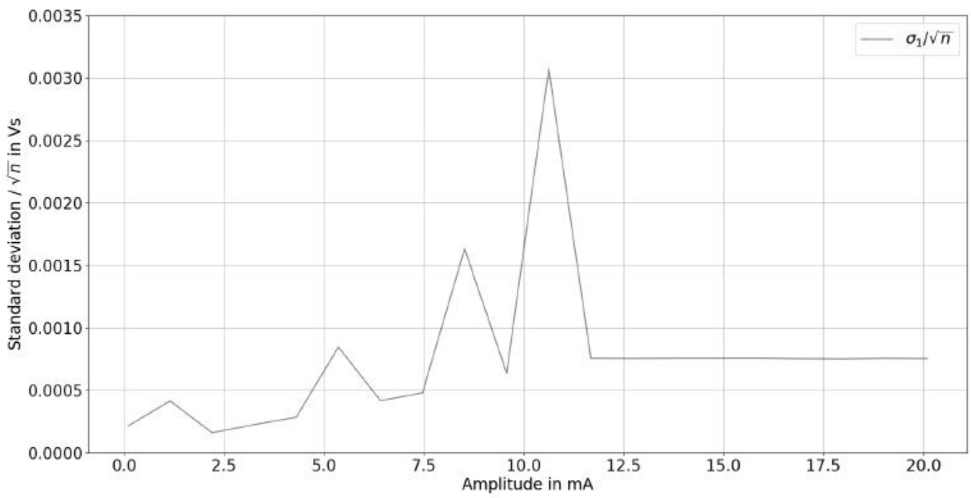

Figure 9.17.: *Standard deviation of the pulse integral of the calibration measurement shown in Figure 9.15 on the old Hardware.*

Compared to the new hardware, the standard deviation is about 10 times larger (see Figure 9.10). Apart from that it is interesting to see that the standard deviation is exactly constant after communication breaks down at 12 mA. To explain this further investigation is needed.

10. Summary

In the previous chapters a method for the absolute calibration of a light source was presented. The light source used was an integrating sphere from Labsphere equipped with three Roithner LaserTechnik UV-LEDs. The set up is controlled with a SBC designed at KIT in Karlsruhe which can be used to set a pulse length and input current on the LEDs of 1-20 μs and 1-20 mA respectively.

The method of calibration consists of two main components. On the one hand, an average absolute measurement with a Hamamatsu calibrated S1331-1010 BQ photodiode is performed while at the same time single pulse measurements with a Hamamatsu R9420-100 PMT are made. The photodiode measurements are taken by a Keithley 6485 picoamperemeter while a 6402 Picoscope records the PMT response. The need for these two measurements arises since the picoamperemeter does not have the time resolution to resolve single pulses at the pulse lengths used. To circumvent this problem the diode is measured with a long integration time of 0.5 s while flashing at 100 Hz to mimic DC while the PMT measurement is used to get single pulse information like the pulse length and integral.

To show that this method works, several measurements on the diode were performed and were presented in subsection 6.1.1. There, the dependence of the measured current on both the pulse length and the input current are investigated and shown to follow a linear trend at input currents higher than 2 mA within 1%.

To analyse the PMT signal, a comparison of three different signal detection algorithms was done. First, was a threshold method which uses a threshold value of 50% of the highest signal value to discriminate between signal and baseline. The second used the variation of a running average to find the start and end of the signal, while the third uses the unsupervised learning algorithm, DB_Scan, to cluster points in the signal and baseline together. The evaluation of these three methods on test data shows that DB_Scan and threshold agree in most of the analysed cases and show a maximum deviation of only ~2% while the running average shows large deviations which indicate problems with the algorithm. Due to the similar performance but much smaller time consumption the threshold method is used to classify pulses.

In order to achieve the necessary level of precision the set up is built of precision machined aluminum profiles with some custom 3D printed parts. This allows for a distance uncertainty of less than 2 mm. To reduce noise on the measurement, the set up is housed in a light tight box which was coated with highly light absorbent paint. In addition, the communication with the flasherboard over wifi was exported to the outside of the box. This allowed for a small uncertainty on the current measurement.

To perform the calibration measurement, a calibration constant is measured which connects the LED input current and pulse length to the number of photons leaving the sphere. This was done by measuring the diode response at LED input currents between 0.1 mA and 10 mA in steps of 0.1 mA and at a pulse length of 5 μs, which was then fit with a linear function. The slope, divided by the 5 μs pulse length, is the calibration constant which is found to be $C_{\text{calib}} = (3.789 \pm 0.002) \cdot 10^8$. In the same measurement, the PMT shows that the pulse area variability at input currents higher than 1 mA is nearly constant and smaller than 1% of the total pulse integral.

When the measured pulse integrals at a flashing rate of 1 Hz and 100 Hz are compared there is a discrepancy of (4.03 ± 0.25)%. Since this is nearly constant for all measurements taken, in the range of 2.66 mA and 3.0 mA a conversion from a 100 Hz measurement to a 1 Hz measurement can be done by subtracting (4.03 ± 0.25)% of the measured value. For different current ranges corrections for this effect can not be done.

The conversion from the measured diode current to a number of photons leaving the sphere is done using the calculated apparent photo efficiency of the photodiode to convert the diode current to a number of photons hitting the diode. By inverting the lambertian light distribution, this flux on the diode can be used to calculate the number of photons emitted by the sphere. This is done by using view factor calculation which are exactly evaluated through heat transfer equations as was shown in chapter 3.

Finally, for the 2.7 mA measurement a full calibration is performed. This value is chosen since it is used for the calibration of the fluorescence detectors. The result of the conversion is $N_{\gamma,\text{Sphere},1\,\text{Hz}} = (4.79 \pm 0.20) \cdot 10^9$. The error on this number corresponds to 4.2% of the measured value which is well within the 5% goal.

From the 22.8.2019 to the 25.8.2019 a team from KIT visited as to perform a hardware upgrade on the sphere from Wuppertal and to obtain calibration measurements on their sphere. In this process, also a comparison between the old and new Hardware was done. In contrast to the sphere from Wuppertal, the KIT sphere includes a 2 in port reducer and it is assumed that this moves the lambertian surface to plane of the port reducer. To maintain the same level of accuracy in the distance, the diode mount was not moved which leads to a new distance from the port to the diode of $d_{\text{new}} = 18.46 \pm 0.2\,\text{mm}$.

On the new hardware a calibration constant of $C_{\text{calib}} = (3.2186 \pm 0.0016) \cdot 10^8$ was measured. This was done on three successive measurements that also show that the run-to-run variation on this constant is smaller than 0.2% and the error margins overlap. The PMT measurements show a pulse area variability of <0.03% of the mean. When the conversion from 100 Hz to 1 Hz is applied the 2.7 mA measurement leads to a photon count of $N_{\gamma,\text{sphere}} = (2.157 \pm 0.083) \cdot 10^9$. This number agrees to within ∼4% with the simulation results obtained using field measurements at the observatory performed by our colleagues at KIT. The old hardware in general shows a worse agreement with the linear fit and a about 10 times higher pulse to pulse variation.

In general the measurement method appears to work well and leads to reasonable numbers of photons per flash. Due to the rigid and simple design the set up is well suited for use in Argentina.

A. Specifications

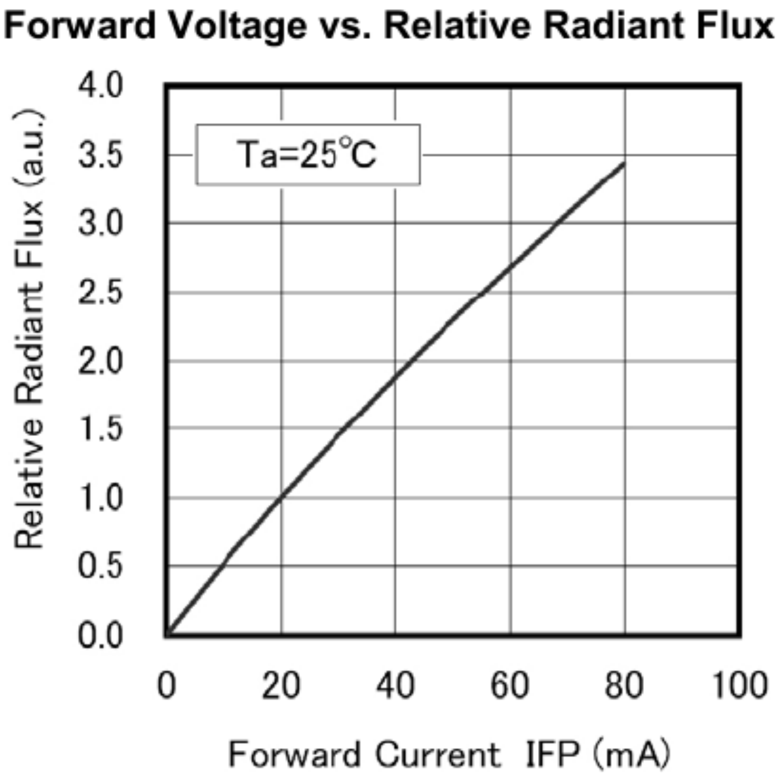

Figure A.1.: *Output photon flux as a function of the input current. In the region between 0 mA and 20 mA it appears to have a small curve. [15]*

B. Measurements

B.1. PMT signal

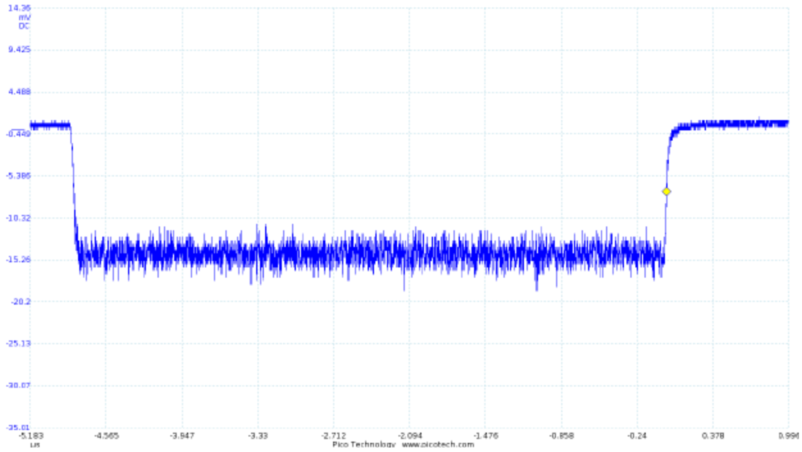

Figure B.1.: *Typical PMT pulse at 3 mA. There is a slope visible in the rising and falling edge.*

B.2. KIT

B.2.1. Calibration measurements

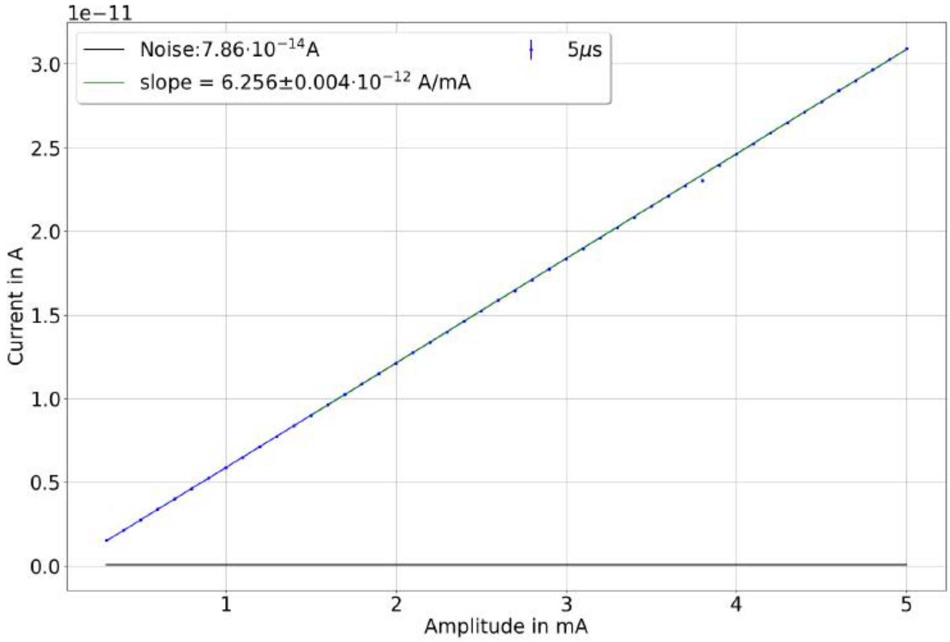

Figure B.2.: *Measurement points with linear fit. Errors are given by* $\frac{\sigma}{\sqrt{n}}$.

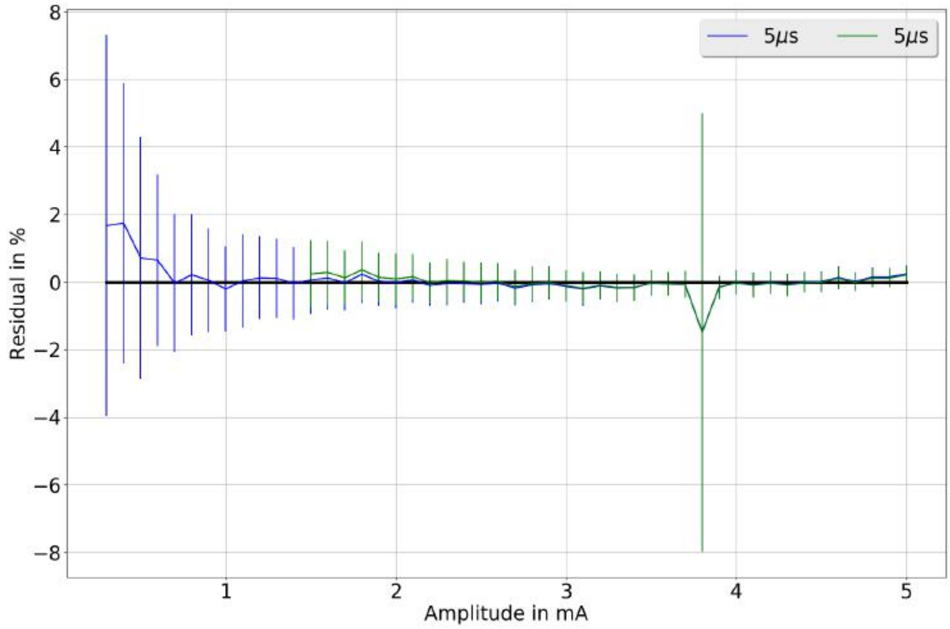

Figure B.3.: *Residuals between the line fit and the data Data points. Errors are given by $\frac{\sigma}{\sqrt{n}}$. Above 2 mA the deviation is <0.5%*

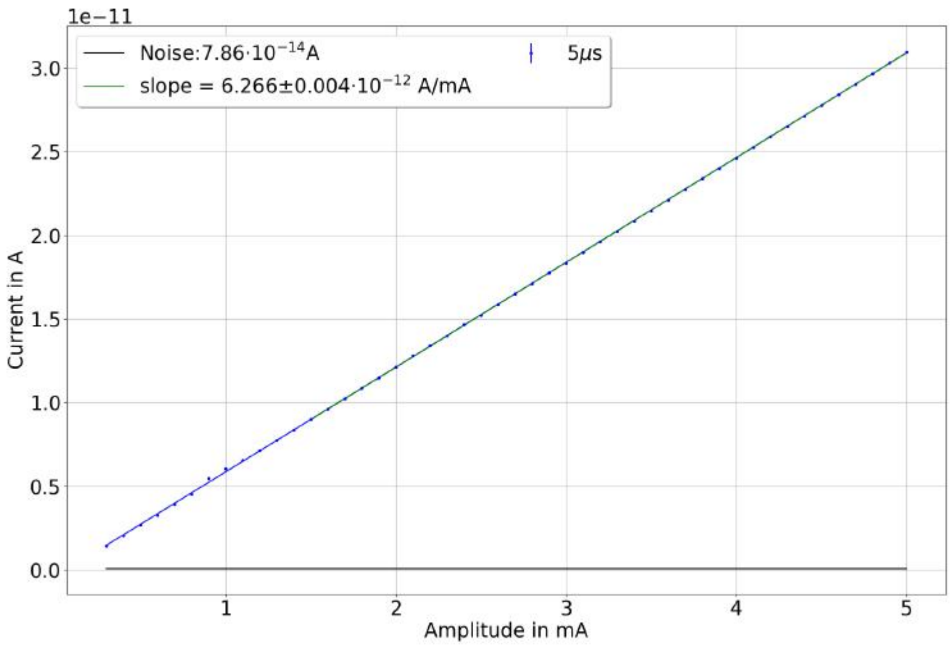

Figure B.4.: *Measurement points with linear fit. Errors are given by $\frac{\sigma}{\sqrt{n}}$.*

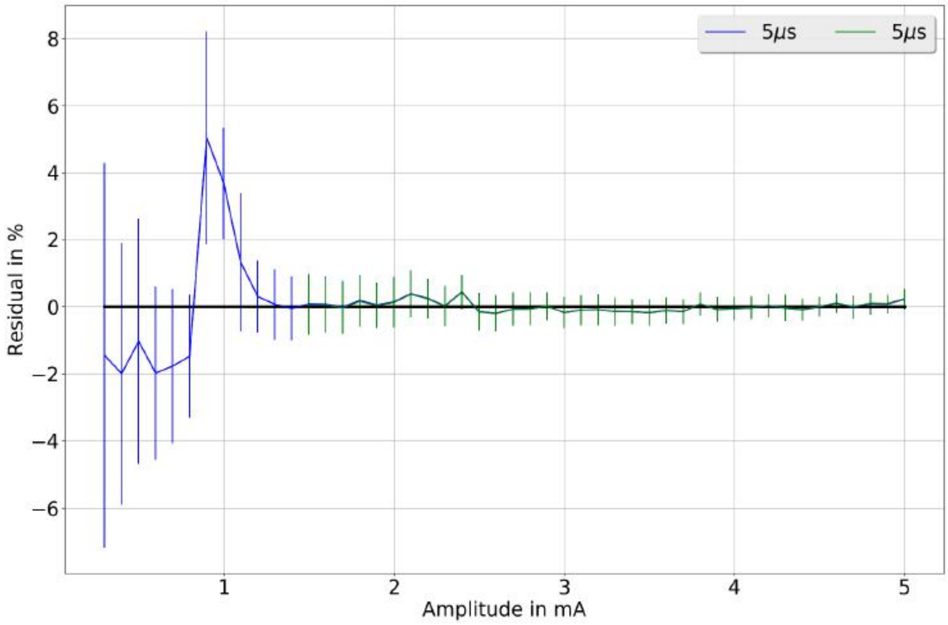

Figure B.5.: *Residuals between the line fit and the data Data points. Errors are given by $\frac{\sigma}{\sqrt{n}}$. Above 2 mA the deviation is <0.5%*

C. Problems in the measurement

C.1. PMT

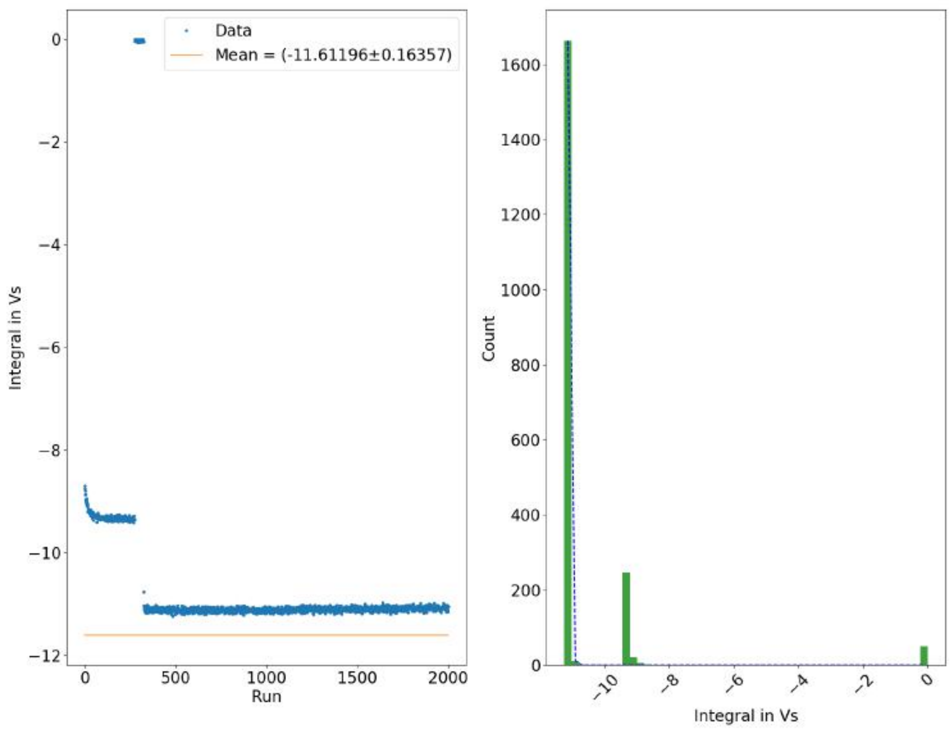

Figure C.1.: *Problematic PMT measurement. At the beginning the Amplitude shows some big jumps. Those could be due to the flasher turning on and off or the Picoscope while starting the measurement.*

Bibliography

[1] Epics. https://epics-controls.org/. Accessed: 2019-09-11.

[2] The pierre auger cosmic ray observatory. *Nuclear Instruments and Methods in Physics Research Section A: Accelerators, Spectrometers, Detectors and Associated Equipment*, 798:172 – 213, 2015.

[3] S Abishek, Srinivasa K Ramanujam, and Subrahmanya S Katte. View factors between disc/rectangle and rectangle in parallel and perpendicular planes. *Journal of thermophysics and heat transfer*, 21(1):236–239, 2007.

[4] CAEN GmbH. *User Manual UM3262;A7501;2100V/100µA High Efficiency HV Power Supply*, rev. 4 edition, 2017.

[5] Hamamatsu Photonics K.K. *Photomultipier Tube R9420*, 12 2014.

[6] Hamamatsu Photonics K.K. *Final Inspection Sheet*, 12 2016.

[7] Wolfram Research, Inc. Mathematica, Version 12.0. Champaign, IL, 2019.

[8] Keithley Instruments, Inc., 28775 Aurora Road, Cleveland, Ohio 44139. *Model 6485 Picoammeter Model 6487 Picoammeter/Voltage Source User's Manual*, 6487-900-01 rev. b edition, 1 2003.

[9] Labsphere. *General Purpose Integrating Spheres*, 2019.

[10] Mathes, Hermann-Josef. A novel method for the absolute end-to-end calibration of the auger fluorescence telescopes. *EPJ Web Conf.*, 210:05013, 2019.

[11] F. Pedregosa, G. Varoquaux, A. Gramfort, V. Michel, B. Thirion, O. Grisel, M. Blondel, P. Prettenhofer, R. Weiss, V. Dubourg, J. Vanderplas, A. Passos, D. Cournapeau, M. Brucher, M. Perrot, and E. Duchesnay. Scikit-learn: Machine learning in Python. *Journal of Machine Learning Research*, 12:2825–2830, 2011.

[12] Pico Technology Ltd., James House Colmworth Business Park ST. NEOTS Cambridgeshire PE19 8YP United Kingdom. *PicoScope 6000 Series;PC Oscilloscopes;User's Guide*, ps6000.en edition, 2009-2011.

[13] Dr. Anna Pollmann. Picogui. personal contact.

[14] Ankit Rohatgi. Webplotdigitizer, 2011. https://apps.automeris.io/wpd/.

[15] Roithner LaserTechnik GmbH, Wiedner Hauptstraße 76, 1040 Vienna, Austria. *UVLED365-110E*, 11 2010.

[16] A.C. Rovero, P. Bauleo, J.T. Brack, J.L. Harton, and R. Knapik. Multi-wavelength calibration procedure for the pierre auger observatory fluorescence detectors. *Astroparticle Physics*, 31(4):305 – 311, 2009.

[17] Roving Networks, Inc., 102 Cooper Court,Los Gatos, CA 95032. *RN-131G & RN-131C 802.11 b/g Wireless LAN Module*, 3.2r edition, 9 2012.

Erklärung

gem § 14 Abs. 7 Prüfungsordnung vom 15.04.2013

Hiermit erkläre ich, dass ich die von mir eingereichte Abschlussarbeit (Bachelor-Thesis) selbständig verfasst und keine anderen als die angegebenen Quellen und Hilfsmittel benutzt sowie Stellen der Abschlussarbeit, die anderen Werken dem Wortlaut oder Sinn nach entnommen wurden, in jedem Fall unter Angaben der Quellen als Entlehnungen kenntlich gemacht habe.

Ort, Datum Unterschrift

Erklärung

Hiermit erkläre ich mich damit einverstanden, dass meine Abschlussarbeit (Bachelor-Thesis) wissenschaftlich interessierten Personen oder Institutionen und im Rahmen von externen Qualitätssicherungsmaßnahmen des Studienganges zur Einsichtnahme zur Verfügung gestellt werden kann.
Korrektur- oder Bewertungshinweise in meiner Arbeit dürfen nicht zitiert werden.

Ort, Datum Unterschrift